MASTER'S DEGREE THESIS

MSc in Applied Mathematics

Title: Methods for solving 1D Stefan problems with application to contact melting.

Author: Michelle De Decker

Advisor: Tim Myers

Tutor: Joan Solà-Morales

Department: Matemàtica Aplicada 1

Institution: Centre de Recerca Matemàtica

Academic year: 2010-2011

Facultat de Matemàtiques i Estadística
UNIVERSITAT POLITÈCNICA DE CATALUNYA

Methods for solving 1D Stefan problems with application to contact melting.

Michelle De Decker
Centre de Recerca Matemàtica

January 31, 2011

Contents

1 Introduction **5**

2 The one dimensional heat equation **6**

2.1 The heat equation with a fixed temperature boundary condition 6

2.1.1 Nondimensionalisation of the problem 6

2.1.2 Exact solution methods 7

2.1.3 Approximate solution methods 8

2.1.4 Results 11

2.2 The heat equation with a constant flux boundary condition 14

2.2.1 Exact solution using the Laplace transform 14

2.2.2 Approximate solutions 14

2.2.3 Results 17

3 One phase Stefan problem **20**

3.1 The nondimensional problem 20

3.2 Exact solution using the similarity variables 21

3.3 Approximate solutions to the Stefan problem 21

3.3.1 Heat balance integral method 22

3.3.2 Refined integral method 22

3.3.3 Optimal exponent heat balance and refined integral method 23

3.3.4 Combined integral method 24

3.3.5 Results 25

3.4 Approximate solutions to the Stefan problem with a large Stefan number 28

3.4.1 The nondimensional problem for large β 28

3.4.2 Perturbation solution 29

3.4.3 Higher order perturbation method 30

3.4.4 Results 31

4 Two phase Stefan problem **37**

4.1 The nondimensional problem 37

4.2 Exact solution using similarity variables 38

4.3 Approximate solutions 38

4.3.1 Optimal heat-balance integral method 38

4.3.2 Optimal refined integral method 39

4.3.3 Results 41

5 3D contact melting **43**

5.1 Introduction 43

5.2 Problem description 43

5.3 Governing equations 44

5.4 Analysis 47

5.5 Results 49

5.6 Application to n-octadecane 54

6 Conclusion **55**

Nomenclature

Table 1: Parameter values for water used in the analysis

h	=	Height of liquid layer	m
h_m	=	Height of melted solid	m
H_0	=	Initial solid height	m
L, W, H	=	Arbitrary length	m
M	=	Mass of solid	kg
n, m	=	Exponents in the temperature profiles	
N	=	Summation integer	
p	=	Pressure	kg m^{-1} s^{-2} (Pa)
s	=	Melt front or Laplacian time	m or s
$\hat{s}$	=	Nondimensional melt front	m
t	=	Time	s
$\hat{t}$	=	Nondimensional time	
T	=	Liquid temperature	K
T_0	=	Substrate temperature	K
T_m	=	Melting temperature	K
T_∞	=	Initial temperature of the liquid	K
u	=	Nondimensional liquid temperature	
$\tilde{u}$	=	Laplace transform of liquid temperature	
v	=	Nondimensional solid temperature	
x, y, z	=	Length	m
$\hat{x}$	=	Nondimensional length	
β	=	Dimensionless inverse Stefan number	
δ	=	Heat penetration depth	m
ϵ	=	Small parameter	
ξ	=	Rescaled length / unit length	m
η	=	Viscosity	kg s^{-1}
θ	=	Solid temperature	K
θ_0	=	Initial temperature of the solid	K
μ	=	Eigenvalue	
ν	=	Nondimensional similarity variable	
τ, $\mathcal{T}$	=	Arbitary time	s

Table 2: Parameter values for water/ice used in the analysis, see [5] and [19].

c_l, c_w	Specific heat in water/ice	4220 / 2050	J kg^{-1} K^{-1}
g	Gravity	9.8	kg s^{-2}
h_{ss}	Heat transfer coefficient between solid and substrate	855	kg s^{-3} K
h_{sl}	Heat transfer coefficient between solid and liquid	763	kg s^{-3} K
k_l, k_s	Thermal conductivity of water/ice	0.571 / 2.18	W m^{-1} K^{-1}
L_m	Latent heat	2.5×10^6	J kg^{-1}
q	Heat flux	0	kg s^{-3}
α_l, α_s	Heat diffusivity of water/ice	1.35×10^{-7} / 1.16×10^{-6}	$[k/\rho c]$
ρ_l, ρ_s	Density of water/ice	1000 / 917	kg m^{-1}

1 Introduction

Contact melting is the process during which a phase change material is placed in contact with a substrate that is at a temperature above the phase change temperature. This leads to melting of the phase change material and a flowing liquid layer which is being squeezed out due to the weight of the solid pushing down upon it. This process arises in many engineering problems such as the production of construction materials and alloys. Other uses include thermal storage systems that rely on the storage of energy as latent heat, which is released upon melting. The mathematical modelling of contact melting involves two heat equations, one in the solid and one in the liquid phase, coupled with the Navier-Stokes equations for the flow in the melt, a Stefan condition at the phase change interface and a force balance between the weight of the solid and the countering pressure in the melt. Consequently, in this thesis we will deal with the one dimensional heat equation and move on to the problem commonly known as the Stefan problem - or moving boundary problem. We will consider both one and two phase problems and eventually look at a contact melting problem. The focus of this dissertation is to develop a three dimensional model to describe a contact melting process and to develop and apply an approximation method with minimal error.

The Stefan problem arises in many physical problems such as melting of ice, aerodynamic ablation, growth of metallic crystals and freezing of food [23]. In some cases the nature of the moving boundary makes it difficult to obtain an exact solution. Very few analytical solutions to Stefan problems exist therefore we need to look for approximate solutions. With the limitation of finding exact solutions, there have been many approximate approaches developed in literature. Analytical methods that have been developed include the heat balance integral method originally put forward by Karman-Pohlhausen [21], which was later adapted by Goodman [9] in his research in phase change materials. This method has been improved by the excellent mathematician Myers [16, 17]. Other analytical methods include the refined integral heat balance [23, 15], similarity, Laplace, perturbation techniques [7, 6], separation of variables and eigenfunction expansions. These methods provide useful solutions to the Stefan problems including solidification of alloys [20], diffusion in grain silos [3], the solidification of a molten material sprayed onto a substrate [14] and temperature in a thermistor [22].

What lacks in the literature is the application of these techniques to contact melting. Bejan's work included the coating of a metallic part with another metal whose melting point is considerably lower [4], while Biance detailed the Leidenfrost effect as a contact melting process [1]. Myers *et al.* [19] developed a two dimensional model for the melting of a rectangular cross-section material on a flat plate. Upon comparison to experimental data provided by Moallemi *et al.* [13] they discovered their model provided a fantastic fit, but with a questionably large heat transfer coefficient.

Our hypothesis is that using a smaller heat transfer coefficient than that used in [19] should provide an equally good fit to the data. We will prove this by considering a three dimensional model and we will apply an approximation method that has minimal error. Furthermore, we will validate our solution by comparison with experimental data provided by Moallemi *et al.*

The structure of this dissertation is designed to take us on a step-by-step exploration of approximate methods for Stefan problems. Whenever possible we will present an exact solution and use this to determine the accuracy of the approximate solutions. The structure is as follows:

- In chapter 2 we deal with the one dimensional heat equation first with a fixed temperature boundary condition and then a constant flux boundary condition.
- In chapter 3 we introduce the one phase Stefan problem and explore the case of both small and large Stefan numbers.
- In chapter 4 we progress to a two phase Stefan problem.

- Finally, in chapter 5 we select and apply the best approximation method to a contact melting problem and validate the solution against experimental data for n-Octadecane.

2 The one dimensional heat equation

2.1 The heat equation with a fixed temperature boundary condition

A 1D semi-infinite material is initially at a temperature T_∞. At $x = 0$ the boundary is heated to a constant temperature T_0. The temperature is then described by,

$$T_t = \alpha T_{xx}, \tag{1}$$

$$T(x, 0) = T_\infty, \tag{2}$$

$$i) \quad T(0, t) = T_0 \quad t \geq 0, \quad ii) \quad T(x, t) \to T_\infty \quad \text{as} \quad x \to \infty. \tag{3}$$

The constant α is the thermal diffusivity defined by $\alpha = \frac{k}{\rho c}$ where k is the thermal conductivity, ρ is the density, c is the specific heat and T denotes the temperature. This system of equations could be used in modelling the heat transferred by conduction through a brick wall or any object made of a homogeneous material, where heat is applied at one end. Using the 1D heat equation a few assumptions are standard:

- The flow of heat only takes place in the $x-$direction.
- The material is insulated (no heat escapes).
- There is no heat generated within the material.
- All the physical quantities (density, specific heat and thermal conductivity) are constant.

These assumptions will carry through all scenarios considered in this report. Where additional assumptions are made they will be stated.

2.1.1 Nondimensionalisation of the problem

We nondimensionalise this problem in order to reduce the parameter space which simplifies the problem. The problem can be nondimensionalised by setting

$$\hat{x} = \frac{x}{L} \quad , \quad \hat{t} = \frac{t}{\tau} \quad \text{and} \quad \hat{u} = \frac{T - T_\infty}{T_0 - T_\infty}, \tag{4}$$

where L and $\hat{u}$ are typical length and temperature scales. The time scale τ is yet to be defined, but will give an indication of the time over which a significant change will occur in the system. The heat equation becomes

$$\hat{u}_{\hat{t}} = \frac{k\tau}{\rho c L^2} \hat{u}_{\hat{x}\hat{x}}. \tag{5}$$

This shows that the time scale for heat flow is

$$\tau = \frac{\rho c L^2}{k}. \tag{6}$$

Using the parameters for water from Table 2 and considering a distance of 1cm, this time scale suggests that a significant increase in $\hat{t}$ will take of the order 420 seconds. Dropping the hats the dimensionless problem is,

$$u_t = u_{xx}, \tag{7}$$

$$u(x, 0) = 0, \tag{8}$$

$$i) \quad u(0, t) = 1, \quad ii) \quad u(x, t) \to 0 \quad \text{as} \quad x \to \infty. \tag{9}$$

Now we will solve this problem exactly using Laplace transforms and similarity variables. Then we will demonstrate how approximate methods can be used and will show how accurate they are. These approximate solutions are needed to solve problems where no exact solution exists, as we will see later in §5

2.1.2 Exact solution methods

Laplace transforms

The Laplace transform of a function $u(x,t)$ for $t > 0$ is defined by the following integral evaluated over $t \in [0, \infty)$:

$$\mathcal{L}\{u(x,t)\} = \int_0^\infty e^{-st} u(x,t) dt = \tilde{u}(x,s), \tag{10}$$

where $\mathcal{L}$ is the Laplace transform and s a complex argument. This transforms the equation from "t-space" to one in "s-space". Using this Laplace operator equation (7) can be reduced to a simple ordinary differential equation (ODE) which is easily solvable,

$$\mathcal{L}\{u_{xx}\} - \mathcal{L}\{u_t\} = 0, \tag{11}$$

and since $u(x,0) = 0$ the governing equation becomes

$$\tilde{u}_{xx} - s\tilde{u} = 0. \tag{12}$$

The transformed boundary conditions are:

$$\tilde{u}(0,s) = \frac{1}{s}, \tag{13}$$

$$\tilde{u}(x,s) \to 0 \quad \text{as} \quad x \to \infty. \tag{14}$$

Equation (12) has the general solution,

$$\tilde{u}(x,s) = Ae^{\sqrt{s}x} + Be^{-\sqrt{s}x}. \tag{15}$$

Condition (14) requires $A = 0$ and (13) gives

$$\tilde{u} = \frac{1}{s} e^{-\sqrt{s}x}. \tag{16}$$

To find u we need an inverse Laplace transform of $\tilde{u}$. An inverse Laplace transform of (16) drops the dependence of s and gives the solution to the original problem,

$$u = \mathcal{L}^{-1}\{\tilde{u}\} = \text{erfc}\left(\frac{x}{2\sqrt{t}}\right), \tag{17}$$

where erfc is the complementary error function [1]. We will use the solution in (17) to verify our approximate solutions.

[1] The complementary error function [26]:

$$\text{erfc}(x) = \frac{2}{\sqrt{\pi}} \int_x^\infty e^{-t^2} dt. \tag{18}$$

Similarity variables

The solution above may also be obtained by the method of similarity variables. Let $u(x,t) = f(\eta)$ where $\eta = Axt^{\alpha}$. Using the chain rule we find

$$u_t = f_\eta \eta_t = f_\eta \alpha A x t^{\alpha-1} \tag{19}$$

$$u_x = f_\eta \eta_x = f_\eta A t^{\alpha} \tag{20}$$

$$u_{xx} = (f_\eta A t^{\alpha})_\eta \eta_x = f_{\eta\eta} A^2 t^{2\alpha} \tag{21}$$

and substituting (19) and (21) into equation (7) we obtain

$$f_\eta \alpha \eta = f_{\eta\eta} A^2 t^{2\alpha+1}. \tag{22}$$

To remove the time dependence we set $\alpha = -1/2$ and then setting $A = 1/\sqrt{2}$ the heat equation simplifies to

$$f_{\eta\eta} = -\eta f_\eta \tag{23}$$

where now $\eta = \frac{x}{\sqrt{2t}}$. Setting $s = f_\eta$, we are left with a first order separable equation,

$$s_\eta = -\eta s, \tag{24}$$

with solution given by

$$\int \frac{1}{s} ds = -\int \eta d\eta = -\frac{1}{2}\eta^2 + C_0 \tag{25}$$

so that $s = f_\eta = C_1 e^{-(\eta/\sqrt{2})^2}$. With a substitution of $\varphi = \eta/\sqrt{2}$ the above becomes a simple first order separable equation

$$df = \sqrt{2} C_1 e^{-\varphi^2} d\varphi \tag{26}$$

which is easily integrated to

$$\begin{aligned} f(\eta) &= A_1 \mathrm{erf}(\varphi) + A_2 \\ &= A_1 \mathrm{erf}\left(\frac{x}{\sqrt{4t}}\right) + A_2. \end{aligned} \tag{27}$$

With $u(x,t) = f(x/\sqrt{2t})$ the boundary conditions (9 i) and (9 ii) correspond to $f(0) = 1$ and $f(\infty) = 0$ respectively. These conditions imply $A_1 = -A_2$ and $A_2 = 1$ which reproduces the solution by Laplace transform in equation (17).

2.1.3 Approximate solution methods

Approximate methods include separation of variables and the heat balance integral method (HBIM). Note that separation of variables is approximate, since we will apply it over a finite domain rather than an infinite domain. In fact, we could also use an eigenfunction expansion rather than separation of variables. In this section we will discuss the separation of variables technique and in the following section we will give an example using an eigenfunction expansion.

Separation of variables

Since this method requires a finite domain the second boundary condition will be considered at $x = L$ where L is large, such that $u(L,t) = 0$. The system (7) - (9) is not homogeneous, so we first make the substitution

$$w(x,t) = u(x,t) - g(x), \tag{28}$$

such that,

$$w(0,t) = 0 \rightarrow g(0) = 1,$$
$$w(L,t) = 0 \rightarrow g(L) = 0.$$

Substitution of (28) into the heat equation (7) gives

$$w_t = w_{xx} + g_{xx}, \tag{29}$$

where $g_{xx} = 0$ is imposed so that we may obtain a homogeneous problem for $w(x,t)$. Applying the boundary conditions we find $g(x) = 1 - x/L$ and the problem is reduced to solving one with homogeneous boundary conditions,

$$w_t = w_{xx}, \tag{30}$$
$$i) \quad w(x,0) = \frac{x}{L} - 1, \quad ii) \quad w(0,t) = w(L,t) = 0. \tag{31}$$

Let $w(x,t) = X(x)T(t)$, then (30) gives

$$\frac{X_{xx}}{X} = \frac{T_t}{T}. \tag{32}$$

For this equation to be true for any choice of x and t we need both sides to be equal to the same constant, which we denote γ. Two ordinary differential equations are obtained:

$$T_t = \gamma T, \tag{33}$$
$$X_{xx} = \gamma X. \tag{34}$$

For $\gamma \geq 0$ we find the trivial solution $\forall\ t,\ x$: $w = 0$. For $\gamma = -\lambda^2 < 0$, where λ is a constant, equation (33) has a solution $T(t) = A_0 e^{\gamma t}$. The spatial equation in (34) is a simple harmonic equation with a general solution $X(x) = C_1 \sin(\lambda x) + C_2 \cos(\lambda x)$. Applying the boundary conditions it is found that $X(0) = X(L) = 0$ such that $C_2 = 0$ and, to avoid a non-trivial solution, $\gamma = -(n\pi/L)^2$ for $n = 1, 2, 3 \ldots$

The general solution to (30) is the summation of all possible solutions that satisfy the boundary conditions:

$$w(x,t) = \sum_{n=1}^{\infty} A_n \sin\left(\frac{n\pi x}{L}\right) e^{-t(n\pi/L)^2}. \tag{35}$$

The initial condition can be expressed as a Fourier series,

$$w(x,0) = \sum_{n=1}^{\infty} A_n \sin\left(\frac{n\pi x}{L}\right) = \frac{x}{L} - 1. \tag{36}$$

Now we multiply this equation through with $\sin\left(\frac{m\pi x}{L}\right)$ and integrate it across the domain $x \in [0, L]$. Making use of the sine orthogonality relation [2] we find the coefficients $A_n = 2/n\pi$. The final step is to add the solution in (35) to $g(x)$ to obtain the separable solution to the heat equation:

$$u(x,t) = \sum_{n=1}^{\infty} \frac{2}{n\pi} \sin(n\pi x/L) e^{-t(n\pi/L)^2} + 1 - x/L. \tag{38}$$

[2] The orthogonality relation of sine [26]:

$$\int_0^L \sin\left(\frac{n\pi x}{L}\right) \sin\left(\frac{m\pi x}{L}\right) = 0 \quad \text{if} \quad m \neq n,$$
$$= \frac{L}{2} \quad \text{if} \quad m = n, \tag{37}$$

Heat balance integral method (HBIM)

The HBIM is an approximation solution method developed by Goodman [9] to solve Stefan problems. In fact, it was simply an application of the earlier Karman-Pohlhausen method for analysing boundary layer flow [21]. Like the separable solution the HBIM is applied over a finite domain although in this case the domain grows in time. To be specific we analyse the problem for $x \in [0, \delta(t)]$ where $\delta(t)$ is termed the heat penetration depth. In this case $\delta(t)$ is defined as the point at which temperature change above the initial temperature is considered negligible (although we do not define what constitutes negligible). So we replace $u \to 0$ as $x \to \infty$ with

$$u(\delta, t) = 0, \tag{39}$$

$$u_x(\delta, t) = 0. \tag{40}$$

The second condition is to ensure the temperature profile joins smoothly with the solution for $x \geq \delta$. The temperature is approximated by a polynomial of the form

$$u = a_0(t) + a_1(t)\left(1 - \frac{x}{\delta}\right) + a_2(t)\left(1 - \frac{x}{\delta}\right)^2. \tag{41}$$

This form is chosen since a constant or linear temperature does not satisfy all boundary conditions ((39), (40)) and so a quadratic is the simplest choice. Applying these conditions we find that $a_0(t) = 0$ and $a_1(t) = 0$, whilst the condition $u(0, t) = 1$ determines $a_2(t) = 1$. The temperature is therefore approximated by

$$u = \left(1 - \frac{x}{\delta}\right)^2, \tag{42}$$

where $\delta(t)$ is still unknown. Note that this form only applies to the region $x \in [0, \delta(t)]$; the solution for $x > \delta(t)$ is assumed to be 0.

To implement the HBIM the heat equation is integrated over the domain $x \in [0, \delta(t)]$ to determine $\delta(t)$;

$$\int_0^\delta u_t dx = \int_0^\delta u_{xx} dx. \tag{43}$$

The derivative can be taken out of the integral using Leibniz's formula for differentiating an integral [3]. Since $u_x(\delta, t) = 0$ and $u(\delta, t) = 0$ it follows that

$$\frac{d}{dt}\int_0^\delta u(x, t) dx = -u_x\Big|_{x=0}. \tag{45}$$

Substitution of the temperature profile in (42) into this integral gives

$$\frac{d}{dt}\int_0^\delta \left(1 - \frac{x}{\delta}\right)^2 dx = \frac{2}{\delta}\left(1 - \frac{x}{\delta}\right)\Big|_{x=0}, \tag{46}$$

which reduces to an ordinary differential equation,

$$\frac{d\delta}{dt} = \frac{6}{\delta}. \tag{47}$$

With the initial condition $\delta(0) = 0$ equation (47) has a solution

$$\delta(t) = \sqrt{12t}. \tag{48}$$

Thus the HBIM solution to the heat equation (7) is

$$u(x, t) = \left(1 - \frac{x}{\sqrt{12t}}\right)^2. \tag{49}$$

[3] Leibniz's formula [5]:

$$\frac{d}{dx}\left[\int_{a(x)}^{b(x)} F(x, m) dm\right] = \int_{a(x)}^{b(x)} \frac{\partial F(x, m)}{\partial x} dm + F(x, b)\frac{db}{dx} - F(x, a)\frac{da}{dx}. \tag{44}$$

2.1.4 Results

A comparison of the approximate solutions with that of the exact solution is shown in Figs. 1(a), 1(b), 1(c). The solid line is the exact solution, the dotted line is the separable solution and the dashed line is the HBIM solution. The solutions are calculated on the spatial domain $x \in [0, 10]$ for $t = 1e^{-7}, 3, 16$s. These times were chosen to capture the solutions most interesting behaviour. In each case two figures are shown: the solution of the temperature profile and the error defined by,

$$E_T = |u_{exact} - u_{approx}|. \tag{50}$$

The main behaviour of the separable solution is captured by the first few terms of the series, although the calculations are shown using 50. Including more terms than this will theoretically increase accuracy, but the computational error may well be of the same order to the amount by which the solution is corrected.

For very early times, shown in Fig. 1(a), the separable solution struggles to deal with the discontinuity imposed by the initial and boundary conditions, i.e. $u(x, 0) = 0$ but $u(0, t) = 1$. This is because the separable solution is being approximated by a sum of continuous functions, i.e. a Fourier series, which will overshoot the solution by approximately 18%. This is known as the Gibbs phenomenon and, in this case, is only a problem in the early time behaviour. In Fig. 1(a) the overshoot is 17.88%, which is not exactly 18% presumably due to rounding error in the computation. The HBIM solution has a very close agreement with the exact solution and is not visibly distinguishable from the exact solution. The error of the HBIM solution is very small so clearly handles early times very well.

Looking at the intermediate time solution in Fig. 1(b) the separable solution, with an error near $4.4e^{-5}$%, is better than the HBIM. Although, the HBIM still offers a good approximation with only a 3.3% error.

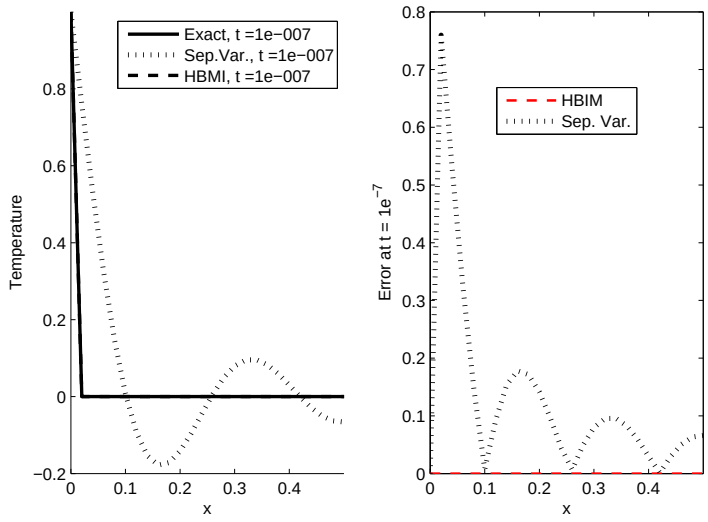

(a) Early time.

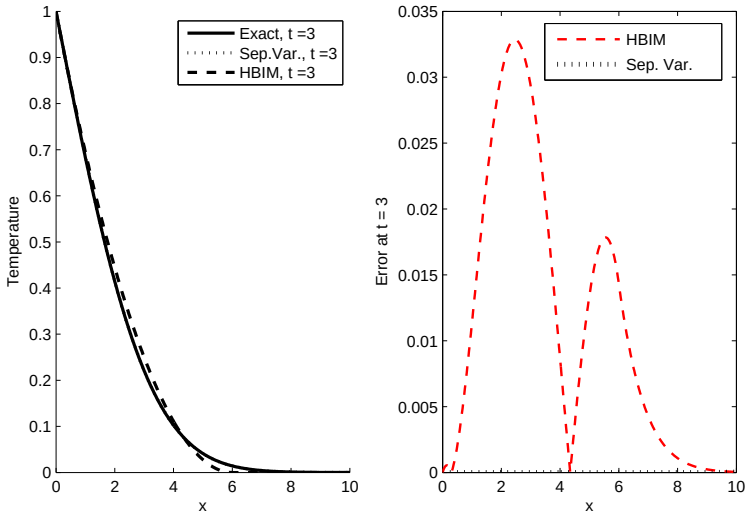

(b) Intermediate time.

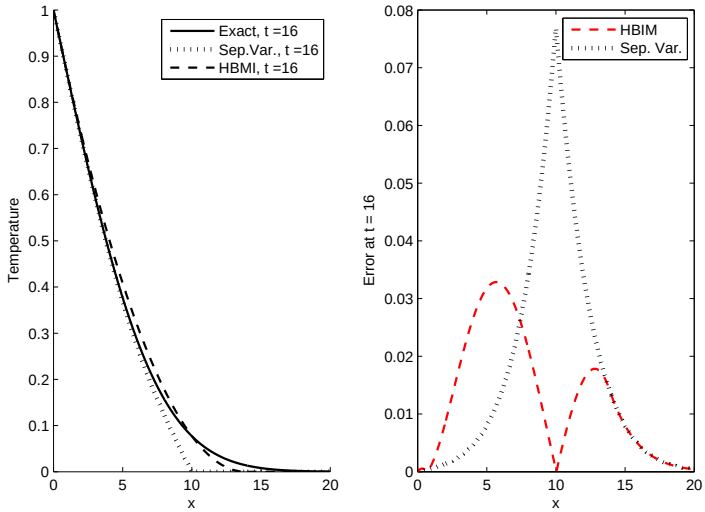

(c) Late time.

Figure 1: Representation of the temperature and error at a different times.

For a late time, shown in Fig. 1(c), the separable solution is bad because the domain is too small for observing the solution at this late time. So, obviously, we should rescale the solution with a larger L. However, this highlights a difficulty with the method since a finite domain needs to be predefined for the separation of variables method to be implemented, i.e. we are required to know where the heat penetration depth is at a specific time. In the case of the HBIM the domain is calculated as part of the solution process and so the same problem does not arise. For times $t = 3, 16$s the approximate penetration depth is $\delta = 6, 13.9$ as shown in Figs. 1(b) and 1(c).

From these solutions we may conclude that the separable solution is good for early times, subsequently care should be taken to ensure the domain is sufficiently large. However, if L is well chosen, provided t is not close to zero, this method is very accurate. The HBIM is valid $\forall t$, its efficiency can be improved (which will be shown later) and there is no issue with choice of domain. However, in general it is less account than separation of variables since the HBIM solution has only one term where as the separable solution can have infinity many terms.

2.2 The heat equation with a constant flux boundary condition

Now we consider the problem with a constant flux condition at the boundary $x = 0$. In the previous section we found that the HBIM performs very well, but we will find that it does not do as well with the constant flux condition. The constant flux problem is expressed by equations (7), (8) and (9 ii) with the new dimensional boundary condition,

$$T_x(0,t) = -Q. \tag{51}$$

Employing a similar nondimensionalisation as in expression (4), but now we nondimensionalise temperature with

$$u = \frac{T - T_\infty}{A}. \tag{52}$$

We find the nondimensional constant flux boundary condition to be

$$u_x(0,t) = \frac{T_x(0,t)}{A} = \frac{-Q}{A}. \tag{53}$$

We want u to be of order 1 so we choose $A = Q$ such that,

$$u_x(0,t) = -1. \tag{54}$$

2.2.1 Exact solution using the Laplace transform

The exact solution can also be found using similarity variables as done in §2.1.2, but the similarity solution gives the same result as Laplace so it is omitted.

Taking the Laplace transform of the problem we obtain equation (12) with a general solution given by (15). The transformed boundary conditions are given by (13) and

$$\tilde{u}_x|_{x=0} = -\frac{1}{s}. \tag{55}$$

Condition (13) gives $A = 0$ and with condition (55) we obtain

$$\tilde{u}(x,s) = s^{-3/2} e^{-\sqrt{s}x}. \tag{56}$$

Taking the inverse Laplace transform of $\tilde{u}$ gives the solution,

$$u(x,t) = \sqrt{\frac{4t}{\pi}} e^{-x^2/4t} - x\text{erfc}\left(\frac{x}{\sqrt{4t}}\right), \tag{57}$$

which will be used to verify our approximate solutions.

2.2.2 Approximate solutions

Eigenfunction expansion

With the change of variable defined by $\hat{x} = L - x$ so $\hat{x} \in [L, 0]$ the problem becomes,

$$u_t = u_{\hat{x}\hat{x}}, \tag{58}$$

with boundary and initial conditions

$$\begin{aligned} &u(0,t) = 0, \\ &\frac{\partial u}{\partial \hat{x}}(\hat{x} = L, t) = -1, \\ &u(\hat{x}, t = 0) = 0. \end{aligned} \tag{59}$$

The reason for this rescaling will become apparent shortly. We assume an eigenfunction expansion solution of the form

$$u(\hat{x},t)=\sum_{n=1}^{\infty}a_n(t)\phi_n(\hat{x}). \tag{60}$$

Multiplying both sides with $\phi_m(\hat{x})$ and integrating over the domain $\hat{x}\in[L,0]$ we obtain

$$\int_L^0 u(\hat{x},t)\phi_m(\hat{x})d\hat{x}=\int_L^0\sum_{n=1}^{\infty}a_n(t)\phi_n(\hat{x})\phi_m(\hat{x})d\hat{x}. \tag{61}$$

We choose $\phi(\hat{x})$ to be the solution to the associated homogeneous ODE with homogeneous boundary conditions:

$$\begin{cases}\phi_{\hat{x}\hat{x}}-\omega\phi=0,\\ \phi(0)=0,\\ \phi_v(L)=0.\end{cases} \tag{62}$$

The only non-trivial solution will be of the form

$$\phi(\hat{x})=A\sin(\lambda\hat{x})+B\cos(\lambda\hat{x}), \tag{63}$$

where $\omega=-\lambda^2$. Applying the boundary conditions in (62) we find $B=0$ and $\cos(\lambda L)=0$. So our eigenfunctions and eigenvalues for the problem described by (58) and (59) are

$$\begin{cases}\phi_n(\hat{x})=\sin(\lambda_n\hat{x}),\\ \omega_n=-\lambda_n^2=-\left(\frac{\pi(2n-1)}{2L}\right)^2 \quad \text{for} \quad n=1,2,\dots\end{cases} \tag{64}$$

If we had used the original x variable we would have obtained an eigenfunction of the form $\phi_n(x)=\cos(\lambda_n x)$ which does not satisfy the flux boundary condition $u_x(x=0,t)=-1$.

Since the eigenfunctions are solutions to the Sturm-Liouville problem they have an orthonormal basis, so

$$\int_L^0\phi_n(\hat{x})\phi_m(\hat{x})d\hat{x}=\frac{L}{2}\delta_{n,m}, \tag{65}$$

where δ is the Kronecker delta[4]. Substituting this into (61) we get an expression for $a_n(t)$,

$$a_n(t)=\frac{2}{L}\int_L^0 u(\hat{x},t)\sin(\lambda_n\hat{x})d\hat{x}. \tag{66}$$

Differentiate with respect to time and noting that $u_t=u_{\hat{x}\hat{x}}$ we obtain,

$$\frac{d}{dt}a_n(t)=\frac{2}{L}\int_L^0 u_{\hat{x}\hat{x}}\sin(\lambda_n\hat{x})d\hat{x}, \tag{67}$$

which can be integrated by parts to get

$$\frac{d}{dt}a_n(t)=\frac{2}{L}\left[-u_{\hat{x}}(L,t)\sin(\lambda_n L)-\lambda_n\int_L^0 u_{\hat{x}}\cos(\lambda_n\hat{x})d\hat{x}\right]. \tag{68}$$

Applying $u_{\hat{x}}(L,t)=-1$ and integrating by parts again we find,

$$\frac{d}{dt}a_n(t)=-\frac{2(-1)^n}{L}-\lambda_n^2\underbrace{\frac{2}{L}\int_L^0 u(\hat{x},t)\sin(\lambda_n\hat{x})d\hat{x}}_{=a_n(t)}, \tag{69}$$

[4]This is defined as

$$\delta_{n,m}=\begin{cases}0, & \text{if} \quad n=m\\ 1. & \text{if} \quad n\neq m\end{cases}$$

which leaves us with an equation for $a_n(t)$:

$$\frac{d}{dt}a_n(t) + \lambda_n^2 a_n(t) + \frac{2(-1)^n}{L} = 0. \tag{70}$$

The solution to the homogeneous equation (70)$\left(\text{i.e. drop off the constant}\frac{2(-1)^n}{L}\right)$ is,

$$a_n(t)_{homo} = Ae^{-\lambda_n^2 t}, \tag{71}$$

where A is a constant. By substitution we can verify that setting the function $a_n(t)$ equal to the constant value $-\frac{2(-1)^n}{L\lambda_n^2}$ will satisfy the non-homogeneous equation. So the particular solution is

$$a_n(t)_{part} = -\frac{2(-1)^n}{L\lambda_n^2}. \tag{72}$$

This leads to the full solution of $a_n(t)$,

$$\begin{aligned} a_n(t) &= a_n(t)_{homo} + a_n(t)_{part} \\ &= Ae^{-\lambda_n^2 t} - \frac{2(-1)^n}{L\lambda_n^2}. \end{aligned} \tag{73}$$

Now we have a solution for $u(\hat{x}, t)$ via (60),

$$u(\hat{x}, t) = \sum_{n=1}^{\infty} \left(Ae^{-\lambda_n^2 t} - \frac{2(-1)^n}{L\lambda_n^2} \right) \sin(\lambda_n \hat{x}). \tag{74}$$

Applying the initial condition $u(\hat{x}, 0) = 0$ we find $A = \frac{2(-1)^n}{L\lambda_n^2}$. Changing the variables back the original $x = L - \hat{x}$ leads us to the solution by eigenfunction expansion,

$$u(x, t) = \sum_{n=1}^{\infty} \frac{2(-1)^n}{L\lambda_n^2} \left(e^{-\lambda_n^2 t} - 1 \right) \sin[\lambda_n (L - x)]. \tag{75}$$

Heat balance integral method

The temperature is assumed to take on the same polynomial form as in equation (41). Applying the conditions $u(\delta, t) = u_x(\delta, t) = 0$ we find $a_0(t) = a_1(t) = 0$, whilst the condition $u_x(0, t) = -1$ determines $a_2(t) = \delta/2$. The temperature is therefore

$$u(x, t) = \frac{\delta}{2} \left(1 - \frac{x}{\delta} \right)^2, \tag{76}$$

where $\delta(t)$ is still unknown.

To solve for $\delta(t)$ we integrate the heat equation over the region $x \in [0, \delta(t)]$ with $u(\delta, t) = u_x(\delta, t) = 0$ giving

$$\frac{d}{dt} \int_0^{\delta} u dx = \left. -u_x \right|_{x=0}. \tag{77}$$

Substituting equation (76) into this expression gives

$$\frac{d}{dt} \int_0^{\delta} \frac{\delta}{2} \left(1 - \frac{x}{\delta} \right)^2 dx = 1, \tag{78}$$

which leads to an ODE in $\delta(t)$, namely

$$\frac{d}{dt} \left(\frac{\delta^2}{3} \right) = 2. \tag{79}$$

With the initial condition $\delta(0) = 0$ equation (79) has the solution,

$$\delta(t) = \sqrt{6t}. \tag{80}$$

Thus the HBIM solution to the heat equation (7) is

$$u(x, t) = \frac{\sqrt{6t}}{2} \left(1 - \frac{x}{\sqrt{6t}} \right)^2. \tag{81}$$

2.2.3 Results

A comparison of the approximate solutions to that of the exact solution is shown in Figs. 2(a), 2(b), 2(c). The solid line is the exact solution, the dotted line is the eigenfunction solution and the dashed line is the HBIM solution. The separable solutions are calculated on the spatial domain $x \in [0, 10]$ for $t = 0.1, 3, 60$s. Note the x-axes are cut off at different points to give a clear representation of the solution. The error of the solution is defined as in (50) and is plotted on the right hand side of the solution in the figures.

At early times, shown in Fig. 2(a), there is a jump discontinuity in the gradient at the boundary $x = 0$. We have defined two temperatures; $\forall x$: $u(x, 0) = 0$ and $\forall t$: $u_x(0, t) = 1$. Like the separable solution in §2.1.4, the eigenfunction solution cannot handle this jump and overshoots it. The error of the eigenfunction solution at $t = 0.1$ is near 100% which is worse than that in the constant boundary condition problem (76%). Since the discontinuity at the boundary is a result of fixing the gradients and not the temperatures, the temperature discontinuity at the boundary is not as big as in §2.1, so the oscillation in the eigenfunction solution is not as big. The HBIM still handles early times better with an error less than 1%. Note the error plot in Fig. 2(a) has been cut off, so we cannot see the maximum value of the eigenfunction error.

However, the eigenfunction solution has a lower error in comparison to the HBIM at intermediate times, as seen in Fig. 2(b). The HBIM error for $t = 3$s sits at 8.5%, which is larger than the 3.5% error in the fixed boundary problem. The HBIM doesn't perform as well for a constant flux problem which serves as motivation to improve the method. This will be done in §3. In Fig. 2(c) we note that the HBIM performs better than the solution by the eigenfunction expansion technique.

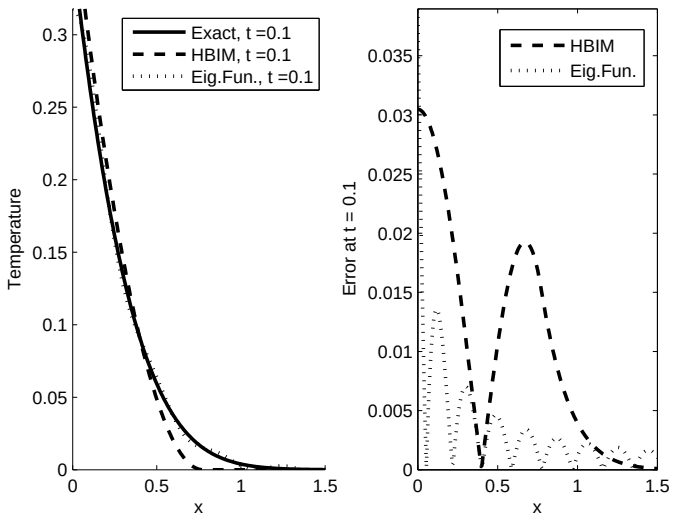

(a) Early time.

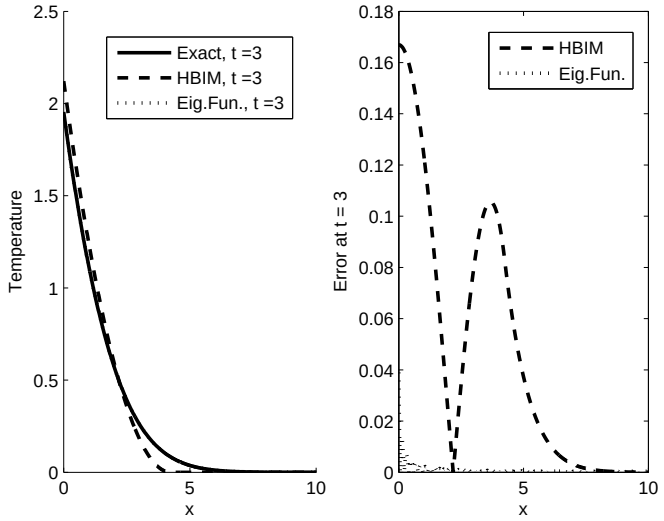

(b) Intermediate time.

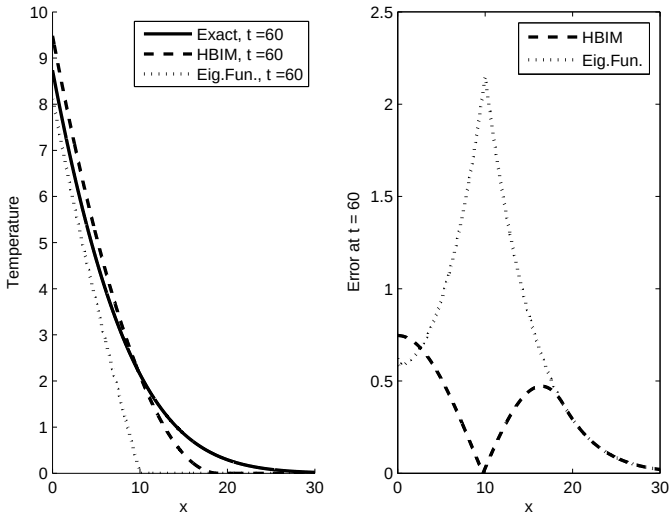

(c) Late time.

Figure 2: Representation of the temperature and error at a different times.

From the results in Figs. 2.1.4 and 2.2.3 we note that the HBIM provides reasonable agreement $\forall t$ and has the advantage over separation of variables in the definition of the domain. However, provided the domain is correctly chosen and t is not close to zero the separable solution is more accurate.

In the following sections we will deal with moving boundaries. Then we find the separable solution is not appropriate. Consequently we will be forced to employ the HBIM, but due to its relative inaccuracy, partially for fixed flux, we will first try to improve it. We will develop the improved combined integral method (CIM), refined integral method (RIM) and optimal exponent approximation methods and apply them to Stefan problems. These approximation methods will also be compared to perturbation and boundary immobilisation approximation methods and, where possible, exact solutions.

3 One phase Stefan problem

Consider the melting of a material initially at the solidus (i.e. at the melting temperature but in a solid state) in the half-plane $x \geq 0$. The material is instantaneously heated to a constant temperature at the boundary $x = 0$ and subsequently melts. Liquid then occupies the region $0 \leq x \leq s(t)$, where $s(t)$ denotes the position of the melt front (the moving boundary) and $s(0) = 0$. The solution of this problem consists of finding the temperature of the liquid, $T(x,t)$, and the position of the moving boundary, $s(t)$.

The problem is governed by the heat equation (1) in the liquid. The initial and boundary conditions are

$$T(x,0) = T_m, \tag{82}$$

$$i) \quad T(0,t) = T_0 \quad ii) \quad T(s,t) = T_m, \tag{83}$$

where T_m is the melt temperature. To determine the domain over which the heat equation holds we require a Stefan condition,

$$\rho L_m \frac{ds}{dt} = -k \frac{\partial T}{\partial x}\bigg|_{x=s(t)} \qquad t \geq 0. \tag{84}$$

Here L_m is the latent heat required to melt the solid and T_0, ρ and k are defined in § 2.1. Equation (84) is an energy balance showing that the energy released through the phase change balances that conducted through the liquid.

3.1 The nondimensional problem

The problem is nondimensionalised by setting

$$\hat{s} = s/X, \quad \hat{x} = x/X, \quad \hat{t} = t/\tau \quad \text{and} \quad \hat{u} = \frac{T - T_m}{T_0 - T_m}. \tag{85}$$

The Stefan condition (84) becomes

$$\frac{\rho L_m X^2}{\tau k \triangle T} \frac{d\hat{s}}{d\hat{t}} = -\frac{\partial \hat{u}}{\partial \hat{x}}\bigg|_{x=s}, \tag{86}$$

where $\triangle T$ is the temperature difference between the two phases, $\triangle T = T_0 - T_m$. The appropriate time scale of heat flow is

$$\tau = \frac{c\rho X^2}{k}, \tag{87}$$

suggesting $x \propto \sqrt{t}$. Using the parameter values from Table 2, this time-scale suggests that it would take of the order 3000s to melt 2cm into the material. The nondimensional governing equation (1) becomes

$$\hat{u}_{\hat{t}} = \frac{\alpha\tau}{X^2} \hat{u}_{\hat{x}\hat{x}}, \tag{88}$$

where

$$\frac{\alpha\tau}{X^2} = \frac{k\tau}{\rho c X^2} = \frac{kc\rho X^2}{\rho c X^2 k} = 1. \tag{89}$$

Dropping the hats the nondimensional problem is described by

$$u_t = u_{xx}. \tag{90}$$

The initial condition (82) and the boundary conditions (83 i) and (83 ii) become

$$u(x,0) = 0, \tag{91}$$

$$i) \quad u(0,t) = 1, \quad ii) \quad u(s,t) = 0. \tag{92}$$

And the Stefan condition (84) becomes

$$\beta \frac{ds}{dt} = - \left. \frac{\partial u}{\partial x} \right|_{x=s} \qquad t \geq 0. \tag{93}$$

where β is the inverse Stefan number, a dimensionless parameter, is defined by

$$\beta = \frac{L_m}{c \triangle T}, \tag{94}$$

where c is the specific heat. The definition of the Stefan number varies depending which book you read. This definition comes from Bejan [5] and Solomon [2]. Other authors such as Hill [12], Fowler [8] have a slightly different definition of $\beta = \frac{c \triangle T}{L_m}$. A large β would require $\triangle T$ to be small which results in a slow melting scenario. Similarly, a small β number means a fast melting scenario.
The problem with a small and large inverse Stefan number will be investigated.

3.2 Exact solution using the similarity variables

Following the same procedure as in §2.1.2 we obtain the solution of equation (90),

$$u(x,t) = A_1 \text{erf}\left(\frac{x}{\sqrt{4t}}\right) + A_2. \tag{95}$$

Imposing boundary conditions (92 i) and (92 ii) we find

$$A_2 = 1, \tag{96}$$

$$A_1 = -1/\text{erf}\left(\frac{s}{\sqrt{4t}}\right). \tag{97}$$

To allow A_1 to be a constant we require $s \propto \sqrt{t}$, so we take

$$s = 2\lambda\sqrt{t}, \tag{98}$$

where λ is an unknown constant. Therefore, the exact solution is

$$u(x,t) = 1 - \frac{\text{erf}(x/\sqrt{4t})}{\text{erf}(\lambda)}. \tag{99}$$

Noting from (98) we have

$$\frac{ds}{dt} = \frac{\lambda}{\sqrt{t}}, \tag{100}$$

and applying the Stefan condition (93) leads to an equation to determine λ:

$$\sqrt{\pi}\beta\lambda e^{\lambda^2}\text{erf}(\lambda) - 1 = 0. \tag{101}$$

So the exact position of the melt front can be expressed by (98) where λ is the root of transcendental equation (101). This will be used to test the accuracy of the approximate solutions.

3.3 Approximate solutions to the Stefan problem

Here we do not use separation of variables because we find the constants in the temperature profile to be a function of time due to the moving boundary, $s(t)$. So we apply integral methods.

3.3.1 Heat balance integral method

The temperature in the domain $x \in [0, s(t)]$, where $s(t)$ is the melt front, is assumed to take on a polynomial form

$$u(x,t) = b_0(t) + b_1(t)\left(1 - \frac{x}{s}\right) + b_2(t)\left(1 - \frac{x}{s}\right)^2. \tag{102}$$

Boundary condition (92 ii) requires $b_0(t) = 0$ and imposing condition (92 i) we find $b_2(t) = 1 - b_1(t)$, therefore

$$u(x,t) = b_1(t)\left(1 - \frac{x}{s}\right) + (1 - b_1(t))\left(1 - \frac{x}{s}\right)^2, \tag{103}$$

where $b_1(t)$ and $s(t)$ are unknown. The coefficient $b_1(t)$ can be found by substituting equation (103) into the Stefan condition (93):

$$\left.\frac{\partial u}{\partial x}\right|_{x=s} = -\frac{b_1(t)}{s} = -\beta\frac{ds}{dt} \tag{104}$$

$$\Rightarrow b_1(t) = \beta s\frac{ds}{dt} \tag{105}$$

To solve for $s(t)$ we integrate the heat equation (90) over the spatial domain $x \in [0, s(t)]$ which gives

$$\frac{d}{dt}\int_0^s u(x,t)dx = u_x(s,t) - u_x(0,t). \tag{106}$$

Note that we could also evaluate $u_x(s,t)$ using the profile (103). Different formulations are discussed in [15, 25], for example we could evaluate $u_x(s,t)$ and $u_x(0,t)$ from (103) or we could let $u_x(s,t) = -\beta s_t$, from the Stefan condition. It was shown in [15] that using the Stefan condition to specify $u_x(s,t)$ is the most accurate, so we will use this formulation. We then calculate $u_x(0,t)$ and the integral of u using (103). This leads to an expression involving ss_t. Replacing this with b_1, through (105), we obtain a quadratic for b_1,

$$b_1^2 + 2(1+6\beta)b_1 - 12\beta = 0. \tag{107}$$

We see from this equation that b_1 is a constant and equation (107) has roots

$$b_1 = -(1+6\beta) \pm \sqrt{(1+6\beta)^2 + 12\beta}. \tag{108}$$

The velocity of $s(t)$ is positive, so to satisfy the Stefan condition we require $u_x(s,t) < 0$. So we can see from (104) we need the positive root of (108). From (105) we have a separable equation for $s(t)$ given by

$$s\frac{ds}{dt} = \frac{1}{\beta}\left(-(1+6\beta) + \sqrt{(1+6\beta)^2 + 12\beta}\right), \tag{109}$$

and with the initial condition $s(0) = 0$ we find

$$s(t) = \sqrt{\frac{2t}{\beta}\left(-(1+6\beta) + \sqrt{(1+6\beta)^2 + 12\beta}\right)}. \tag{110}$$

Once we know $s(t)$ and b_1 we know the temperature for all time through equation (103). As seen in literature the HBIM has questionably accuracy [15], so we introduce the refined integral method as an improvement. We will also discuss further improvements to both HBIM and RIM in the following sections.

3.3.2 Refined integral method

Again we analyse the temperature in the domain $x \in [0, s(t)]$ and we assume the profile in (103) with b_1 constant in time as defined in (105). Now we integrate the heat equation (90) twice to give

$$\int_0^s\int_0^x \frac{\partial u}{\partial t}dydx = \int_0^s u_x(x,t) - u_x(0,t)dx. \tag{111}$$

Integrating the left hand side by parts and with $u(s,t)=0$ and $u(0,t)=1$ equation (111) reduces to

$$\left[x\int_0^x u_t dy\right]\Bigg|_0^s - \int_0^s x u_t dx = -1 - s u_x(0,t). \tag{112}$$

Using $u_t = u_{xx}$ the left hand side can be expanded,

$$s u_x(s,t) - s u_x(0,t) - \int_0^s x u_t dx = -1 - s u_x(0,t). \tag{113}$$

The terms $s u_x(0,t)$ cancel out and using the Stefan condition (93) the expression simplifies to

$$\frac{d}{dt}\int_0^s x u dx = 1 - s\beta\frac{ds}{dt}. \tag{114}$$

In this evaluation, unlike in the HBIM, we avoid evaluating the derivative of the unknown function $u_x(0,t)$. Substituting (105) and (103) into (114) gives a quadratic in b_1,

$$b_1^2 + (1+6\beta)b_1 - 6\beta = 0, \tag{115}$$

which has a positive root that satisfies the Stefan condition:

$$b_1 = \frac{1}{2}\left(-(1+6\beta) + \sqrt{(1+6\beta)^2 + 24\beta}\right). \tag{116}$$

From (105) we have a separable equation for $s(t)$ with solution

$$s(t) = \sqrt{\frac{t}{\beta}\left(-(1+6\beta) + \sqrt{(1+6\beta)^2 + 24\beta}\right)}. \tag{117}$$

Once we know $s(t)$ and b_1 we know the temperature for all time through equation (103).

3.3.3 Optimal exponent heat balance and refined integral method

There is a lot of debate about the choice of the approximating function of $u(x,t)$. Myers [17] proposed a function of the form

$$u(x,t) = a\left(1 - \frac{x}{s}\right) + (1-a)\left(1 - \frac{x}{s}\right)^n, \tag{118}$$

where n is unknown. The problem now involves three unknowns, a, n and s, where a is a constant, n is the optimal exponent (also constant) and s the moving boundary. The key of the method of [17] is to introduce another equation so that n is chosen to minimise the error defined by,

$$E_n(t) = \int_0^s \left[\frac{\partial u}{\partial t} - \frac{\partial^2 u}{\partial x^2}\right]^2 dx = \int_0^s f^2 dx \geq 0, \tag{119}$$

an additional equation is provided to determine the extra parameter n. With the introduction of the error function we can measure the accuracy of the method without knowing the exact solution to the problem. The parameter n is determined by minimizing the least-squares error in (119). If u is an exact solution then $E_n = 0$, otherwise we get $E_n > 0$. Although the choice of E_n has complicated algebra associated with it, it assures that a best fit over all of the domain is found, not just at the boundaries.

For the HBIM we follow the same procedure as that in §3.3.1 and obtain the Stefan condition,

$$\beta\frac{ds}{dt} = \frac{a}{s}, \tag{120}$$

which leads to a solution for the position of the melt front,

$$s(t) = \sqrt{\frac{2at}{\beta}}. \tag{121}$$

Substituting this expression for $s(t)$ into the Stefan condition (120) we obtain quadratic equation that a satisfies,

$$\frac{2(n+1)(a+(1-a)n)}{2+an-a+2\beta(n+1)} = \frac{a}{\beta}. \tag{122}$$

Since both t, $\beta > 0$ we see from (121) that we require $a > 0$ so the melt front velocity is positive. With a and s known in terms of n and β we can calculate the error function $E_n(t)$. Using the temperature profile (118) we obtain an expression for the error,

$$E_n(t) = \frac{a^2 s_t^2}{9s} + \frac{(a-1)^2 n s_t^2}{s(4n^2-1} + \frac{n^2(n-1)^2(a-1)^2}{s^3(2n-3)} - \frac{4as_t^2(a-1)}{s(n+2)(n+1)} + \frac{2(a-1)as_t}{s^2} - \frac{n^2 s_t (a-1)^2}{s^2(2n-1)}. \tag{123}$$

Note that $n = 0.5, 1, 1.5$ are not considered as they result in an infinite error. As argued in [17] and evident in (123), it is found that $E_n = e_n t^{-3/2}$ and the minimum value of e_n depends on n and β, not t. Since E_n decays with time we expect the approximating methods to increase in accuracy as time increases.

A similar analysis holds for minimising the error with the optimal RIM, with the change that (122) is replaced by

$$\frac{3(n+2)(n+1)}{3an+an^2-4a+6+3\beta(n+1)(n+2)} = \frac{a}{\beta}. \tag{124}$$

Knowing what a, s and n are we can find the temperature for all time via (118).

3.3.4 Combined integral method

A method put forward by Mitchell & Myers [24] is to implement the HBIM with an unknown exponent and introduce another equation to determine n by using the RIM. The algebra to determine n is simpler than with the optimal exponent method and the accuracy can be checked using E_n. It turns out that the solution obtained by the CIM will always be as accurate or more accurate than the better of the RIM and HBIM solutions with $n = 2$. [24].

To implement the CIM the temperature assumes a profile as in (118) and we integrate the heat equation (90) over $x \in [0, s]$ as for the HBIM to give (106). Substituting the temperature profile into this expression gives

$$s\frac{ds}{dt} = \frac{2n(n+1)(1-a)}{a(n+1)+2(1-a)}. \tag{125}$$

The Stefan condition can be written as (120) with a melt front solution (121).

To determine n we obtain another equation by implementing the RIM. Integrating the heat equation (90) twice gives (113) where the $u_x(s,t)$ terms cancel out. Substituting for u from (118) we obtain

$$s\frac{ds}{dt} = \frac{3(1-a)(n+1)(n+2)}{a(n+1)(n+2)+6(1-a)}. \tag{126}$$

The idea of the CIM is to combine the HBIM and RIM by equating equations (125) and (126). Using the Stefan condition to eliminate ss_t we obtain an expression of a:

$$a = \frac{6(2-n)}{(n-1)(2n^2+5n-6)}. \tag{127}$$

To determine n we substitute (127) and the Stefan condition (120) into (125) and obtain

$$2n(n+1)[\beta(2n-3)(2+n)(1+n)(2n^2+5n-6)+12(n-2)]=0. \tag{128}$$

The approximate value of n is that which satisfies this equation. The unrealistic values $n=0,-1$ are not considered and since we require $a>0$ we note, from (127), that $n\in(1,2)$. With $\beta>0$ equation (128) restricts $n\in[1.5,2)$. The quintic equation for n (after eliminating the factor $n(n+1)$) may be easily solved numerically. Once n is known all other parameters may be calculated.

3.3.5 Results

The HBIM and RIM solutions are simple to compute, whilst the exact solution requires the evaluation of the Gauss error function. To solve for λ in equation (101) the function $fzero$ is used in Matlab. The temperature profiles shown in the following figures are those at $t=0.1$, which corresponds to approximately 5 minutes on the dimensional scale. This is calculated via equation (87) with parameters values taken from Table 2. The solutions are calculated on the domain $x\in[0,0.4]$ with $\beta=1$. It was shown by Myers that the error of RIM method peaks at $\beta=1$, so in fact we will be considering the worst case scenario. Using any other value of β will result in a more accurate RIM result. We find the minimum of e_n and the corresponding value of n are $(0.075,1.769)$ and $(0.077,1.790)$ for the HBIM and the RIM respectively. We will use these values. Moreover, these arbitrary domain and parameter values are chosen so we have interesting results.

In Fig. 3(a) the temperature profile predicted by the exact solution (solid line) is compared to the HBIM with $n=2$ and $n=1.769$ (dashed and dot-dash lines) and RIM with $n=2$ and $n=1.790$ (black and green dotted lines). On the right hand side of the figure the associated error defined by equation (50) is plotted.

The melt front is shown in Fig. 3(b) with the same legend as that in Fig. 3(a). The time axis runs up to $t=8$ which is approximately 6.5 hours on the dimensional scale. The error of the position of the melt front is plotted on the right hand side and defined by

$$E_s=|s_{exact}-s_{approx}|. \tag{129}$$

The relative error is independent of time since the exact solution and all integral methods have a melt front solution of the form $s\propto\sqrt{t}$. So the relative error will reflect the different predictions of the constant a in (121).

The RIM with $n=1.790$ predicts both the melt front and temperature profile with less error than that of the other approximation methods. In both the temperature and the melt front solutions the error in the RIM (HBIM) with $n=1.790$ (1.769) is lower than that with $n=2$ (2).

Furthermore, the predicted melt front positions will match the exact solution well near $t=0$ since we have the condition $s(0)=0$. The melt front moves away from $x=0$ as time progresses. Initially $s(t)$ moves quickly with time, but the $s(t)$ graph starts leveling off since $s\propto\sqrt{t}$.

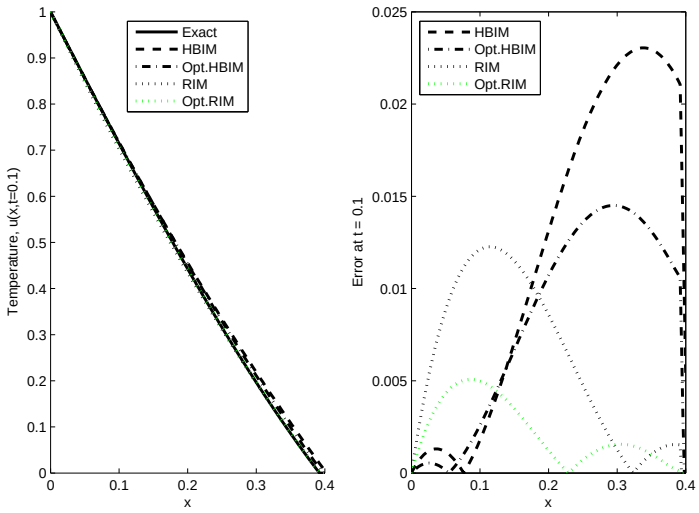

(a) Representation of u(x,0.1) and the error of the approximate solutions compared to the exact.

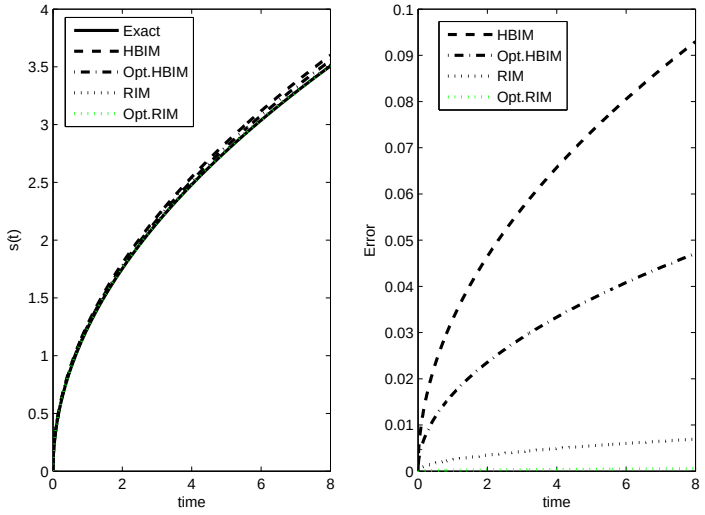

(b) Representation of the melt front and corresponding error.

Figure 3: Plots of the exact solution (solid line), the HBIM with $n = 2$ and $n = 1.769$ (dashed and dot-dash lines) and RIM with $n = 2$ and $n = 1.790$ (black and green dotted lines)

In Fig. 4(a) the temperature profile predicted by the exact solution (solid line) is compared to the HBIM with $n = 1.769$ (dashed line), RIM with $n = 1.790$ (dot-dashed line) and CIM with $n = 1.546$ (dotted line), with associated error defined by equation (50) on the right hand side. In Fig. 4(b) the melt front is shown with the same legend as that in Fig. 4(a) with the error defined by (129) along side. Again, the temperature profile is shown at $t = 0.1$ and the melt front is plotted up to $t = 8$.

The CIM solution will always be as accurate as the better prediction of the RIM and HBIM with $n = 2$ and will usually better both [24], and we also noted from Figs. (3(a),3(b)) that the optimal exponent integral methods perform better than those with $n = 2$. For these reasons the CIM is only compared to the optimal exponent cases, as seen in Figs. (4(a), 4(b)). We note from this analysis that the RIM with $n = 1.790$ has a lower error in both the temperature profile and the melt front predictions.

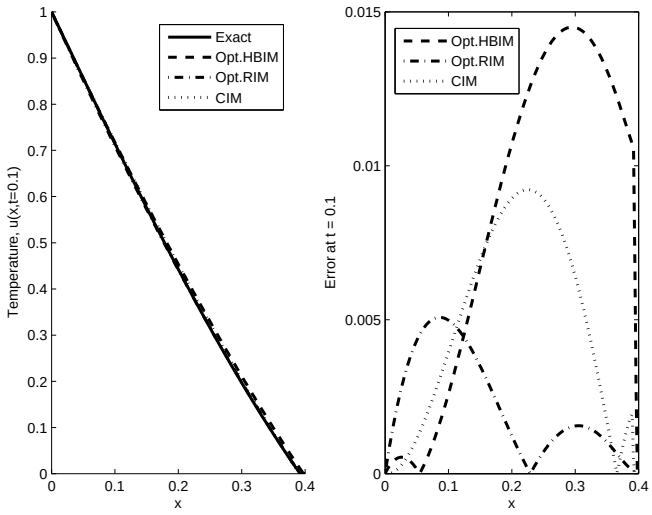

(a) Representation of u(x,0.1) and the error of the approximate solutions compared to the exact.

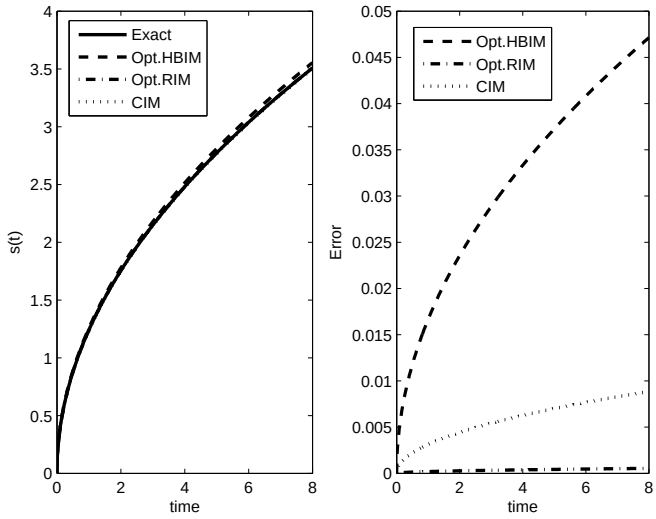

(b) Representation of the melt front and corresponding error.

Figure 4: Plots of the exact solution (solid line), optimal exponent HBIM (dashed line), optimal exponent RIM (dot-dashed line) and the CIM (dotted line).

In fact, the most important quantity of the Stefan problem is the position of the melt front. Here we report the percentage errors of the predicted melt front by the integral methods:

Percentage errors of s(t), where $\beta = 1$.		
RIM	$n = 2$	0.2%
	$n = 1.790$	0.015%
HBIM	$n = 2$	2.65%
	$n = 1.769$	1.34%
CIM	$n = 1.546$	0.25%

Based on these errors, we select the three methods with the lowest error and compare them over the range $\beta \in [0, 1]$. In Fig. 5 we have plotted the logarithm of the relative error the RIM with $n = 2$ (solid line), the optimal RIM (dashed line) and CIM (dot-dashed line) against the β values. The exponent for the optimal RIM

and the CIM will depend on the β value and is determined via equations (123) and (128) respectively. The RIM performs better than the CIM for $\beta < 0.04$ contradicting Myers [24], but the optimal RIM method offers a solution with the lowest error for all β values in this range.

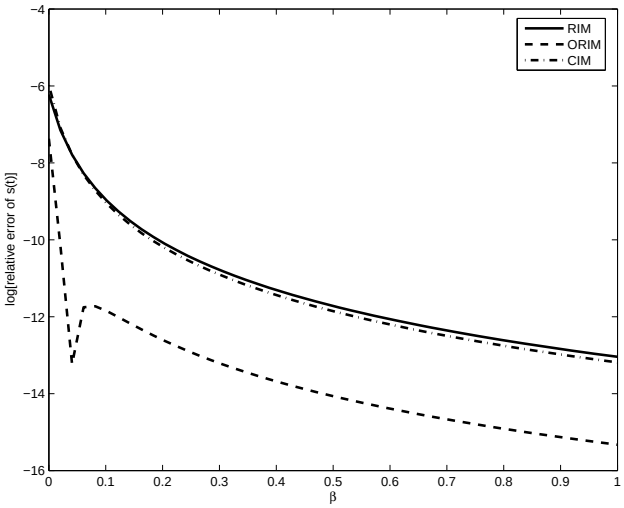

Figure 5: Comparison of the logarithm of the relative errors of the RIM with $n = 2$ (solid line), the optimal RIM with $n = 1.790$ (dashed line) and CIM with $n = 1.546$ (dot-dashed line).

When we move on to solving the two phase Stefan problem we should opt for the use of the optimal exponent RIM. But depending on the ease of implementation and level of accuracy we require we could choose any of the methods explored here, as they all have an error less than 3%. Before we move on to the two phase problem we would like to see how these integral methods behave when β is large.

3.4 Approximate solutions to the Stefan problem with a large Stefan number

Now that we have a small parameter in the governing equation we can use standard perturbation theory to find approximate solutions.

3.4.1 The nondimensional problem for large β

If we consider the case of large β we can rescale the problem such that there is a small parameter in the governing equation. Then we can apply standard perturbation theory to the problem and compare the results with the approximate solutions of the integral methods.

The inverse Stefan number is as defined before, but now we consider $\beta \gg 1$ which means $\triangle T \ll 1$. That is, the temperature gradient driving the melting must be small and therefore we expect slow melting. This can be seen in the Stefan condition (93) where, if we define $\epsilon = 1/\beta$ then $\frac{ds}{dt} = \mathcal{O}(\epsilon)$ and so s_0, the leading order in ϵ, is zero. To follow the progression of the front we need to work on a different time scale.

We choose a time-scale that will balance the Stefan condition in (93). An obvious choice is

$$\hat{t} = \epsilon t, \tag{130}$$

which results in a Stefan condition for the large β case to be (dropping the hat notation)

$$\frac{ds}{dt} = -\left.\frac{\partial u}{\partial x}\right|_{x=s(t)} \qquad t \geq 0. \tag{131}$$

and the governing equation (90) becomes

$$\epsilon u_t = u_{xx}, \tag{132}$$

with initial condition (91) and boundary conditions (92 i) and (92 ii).

3.4.2 Perturbation solution

The solution is approximated by a power series in the small parameter ϵ:

$$u(x,t) = u_0(x,t) + \epsilon u_1(x,t) + \epsilon^2 u_2(x,t) + \dots \tag{133}$$

where $s(t)$ and u_0, u_1, u_2, etc. are unknown. The governing equation (132) becomes

$$\epsilon(u_{0t} + \epsilon u_{1t} + \epsilon^2 u_{2t} + \dots) = u_{0xx} + \epsilon u_{1xx} + \epsilon^2 u_{2xx} + \dots \tag{134}$$

Grouping terms with the same power of ϵ we get a series of differential equations:

$$\epsilon^0 : \qquad u_{0xx} = 0, \tag{135}$$

$$\epsilon^1 : \qquad u_{1xx} = u_{0t}, \tag{136}$$

$$\epsilon^2 : \qquad u_{2xx} = u_{1t}, \tag{137}$$

$$\vdots \tag{138}$$

Similarly, substituting (133) into boundary conditions (92 i) and (92 ii) we get

$$u_0(0,t) + \epsilon u_1(0,t) + \epsilon^2 u_2(0,t) + \dots = 1 \quad \Rightarrow \quad u_0(0,t) = 1, \quad u_i(0,t) = 0 \quad \text{for} \quad i = 1,2,3,\dots \tag{139}$$

$$u_0(s,t) + \epsilon u_1(s,t) + \epsilon^2 u_2(s,t) + \dots = 0 \quad \Rightarrow \quad u_i(s,t) = 0 \quad \text{for} \quad i = 0,1,2,\dots \tag{140}$$

Equation (135) has the general solution $u_0 = A(t)x + B(t)$. Condition (139) requires $B(t) = 1$ and (140) gives the leading order solution,

$$u_0(x,t) = 1 - \frac{x}{s}. \tag{141}$$

Knowing the solution of u_0 we find equation (136) has the general solution $u_1 = \frac{x^3 s_t}{6s^2} + C(t)x + D(t)$. Condition (139) requires $D(t) = 0$ and (140) gives the first order solution,

$$u_1(x,t) = \frac{x s_t}{6s^2}\left(x^2 - s^2\right). \tag{142}$$

So we find the perturbed solution to the first order to be

$$u(x,t) = 1 - \frac{x}{s} + \epsilon\frac{x s_t}{6s^2}\left(x^2 - s^2\right). \tag{143}$$

Substituting for u, defined by (143), leads to

$$\frac{ds}{dt} = \; -\left(u_{0x} + \epsilon u_{1x}\right)\Big|_{x=s(t)}. \tag{144}$$

This may be written as,

$$s\frac{ds}{dt} = \left(1 + \frac{\epsilon}{3}\right)^{-1}. \tag{145}$$

Solving this gives $s(t) = \sqrt{\frac{6t}{3+\epsilon}}$. Taking the Maclaurin [5] series of this function up to order $\mathcal{O}(\epsilon)$ gives the solution of $s(t)$ to the first order,

$$s(t) = \sqrt{2t}\left(1 - \frac{\epsilon}{6}\right). \tag{146}$$

[5] A Maclaurin series is a Taylor series expansion of a function about 0, i.e. $f(x) = f(0) + \frac{f'(0)}{1!}x + \frac{f''(0)}{2!}x^2 + \frac{f^{(3)}(0)}{3!}x^3 \dots$

This is as far as we may take the perturbation. When solving for u_2 we have it in terms of s_{tt}, but we only have one initial condition for $s(t)$. Therefore we are restricted to a first order approximation of u. To find a higher order approximation of u we need to solve the problem making use of a boundary immobilisation then using a perturbation method.

3.4.3 Higher order perturbation method

By introducing a change of variable the moving boundary is fixed. We define $\xi = \frac{x}{s}$ and consider $u(x,t) = v(\xi,t)$. With this change of variable the boundary conditions in (92 i) and (92 ii) become

$$v(0,t) = 1, \tag{147}$$

$$v(1,t) = 0, \tag{148}$$

which specifies a fixed domain $\xi \in [0,1]$. To find the governing equation we need to compute the derivatives using the chain rule:

$$\frac{\partial u}{\partial x} = \frac{1}{s}\frac{\partial v}{\partial \xi}, \tag{149}$$

$$\frac{\partial^2 u}{\partial x^2} = \frac{1}{s^2}\frac{\partial^2 v}{\partial \xi^2}, \tag{150}$$

$$\frac{\partial u}{\partial t} = \frac{\partial v}{\partial \xi}\frac{\partial \xi}{\partial t} + \frac{\partial v}{\partial t}, \tag{151}$$

where

$$\frac{\partial \xi}{\partial t} = \frac{\partial}{\partial t}\left[\frac{x}{s}\right] = -\frac{x s_t}{s^2} = -\frac{\xi s_t}{s}. \tag{152}$$

The Stefan condition in (131) can be written as

$$\frac{\partial s}{\partial t} = -\frac{1}{s}\left.\frac{\partial v}{\partial \xi}\right|_{\xi=1}. \tag{153}$$

Substituting (150)-(153) into (132) we obtain the governing equation,

$$\epsilon\left[\xi v_\xi|_{\xi=1}\, v_\xi + s^2 v_t\right] = v_{\xi\xi}. \tag{154}$$

The solution of (154) is approximated by a power series in the small parameter ϵ,

$$v(\xi,t) = v_0(\xi,t) + \epsilon v_1(\xi,t) + \epsilon^2 v_2(\xi,t) + \ldots, \tag{155}$$

where $s(t)$ and v_0, v_1, v_2, etc. are unknown. The governing equation (154) becomes

$$\begin{aligned}&\epsilon\left[\xi(\, v_{0\xi}|_{\xi=1} + \epsilon\, v_{1\xi}|_{\xi=1} + \epsilon^2\, u_{2\xi}|_{\xi=1} + \ldots)(v_{0\xi} + \epsilon v_{1\xi} + \epsilon^2 u_{2\xi} + \ldots) + s^2(v_{0t} + \epsilon v_{1t} + \epsilon^2 u_{2t} + \ldots)\right]\\ &= v_{0\xi\xi} + \epsilon v_{1\xi\xi} + \epsilon^2 v_{2\xi\xi} + \ldots\end{aligned} \tag{156}$$

Grouping terms of equal powers in ϵ we obtain:

$$\epsilon^0: \quad v_{0\xi\xi} = 0, \tag{157}$$

$$\epsilon^1: \quad v_{1\xi\xi} = \xi\, v_{0\xi}|_{\xi=1}\, v_{0\xi} + s^2 v_{0t}, \tag{158}$$

$$\epsilon^2: \quad v_{2\xi\xi} = \xi(\, v_{0\xi}|_{\xi=1}\, v_{1\xi} + v_{1\xi}|_{\xi=1}\, v_{0\xi}) + s^2 v_{1t}, \tag{159}$$

$$\vdots$$

Similarly, substituting (155) into boundary conditions (92 i) and (92 ii) we get

$$v_0(0,t) + \epsilon v_1(0,t) + \epsilon^2 v_2(0,t) + \ldots = 1 \quad \Rightarrow \quad v_0(0,t) = 1, \quad v_i(0,t) = 0 \quad \text{for} \quad i = 1,2,3,\ldots \tag{160}$$

$$v_0(1,t) + \epsilon v_1(1,t) + \epsilon^2 v_2(1,t) + \ldots = 0 \quad \Rightarrow \quad v_i(1,t) = 0 \quad \text{for} \quad i = 0,1,2,\ldots \tag{161}$$

Equation (157) has the general solution $v_0 = A(t)\xi + B(t)$. Condition (160) requires $B(t) = 1$ and (161) gives the leading order solution,

$$v_0(\xi, t) = 1 - \xi, \tag{162}$$

which is independent of t. Since $v_{0\xi} = -1$ and $v_{0t} = 0$ the equation for v_1 in (158) becomes

$$v_{1\xi\xi}(\xi, t) = \xi, \tag{163}$$

which has a general solution $v_1 = \frac{1}{6}\xi^3 + A(t)\xi + B(t)$. Condition (160) requires $B(t) = 0$ and (161) gives the first order solution:

$$v_1(\xi, t) = \frac{\xi}{6}\left(\xi^2 - 1\right). \tag{164}$$

The second order equation becomes

$$v_{2\xi\xi}(\xi, t) = -\frac{\xi}{2}\left(\xi^2 + \frac{1}{3}\right), \tag{165}$$

since $v_{1t} = 0$. Solving this with the boundary conditions in (160) and (161) gives the second order solution:

$$v_2(\xi, t) = -\frac{\xi^5}{40} - \frac{\xi^3}{36} + \frac{19\xi}{360}. \tag{166}$$

Substituting the second order perturbation correction of v, i.e. $v_0 + \epsilon v_1 + \epsilon^2 v_2$, into the Stefan condition (153), gives

$$s(t) = \sqrt{2t\left(1 - \frac{\epsilon}{3} + \frac{7\epsilon^2}{45}\right)}. \tag{167}$$

Taking the expansion of this function up to order $\mathcal{O}(\epsilon^2)$ gives the solution of $s(t)$ to the second order,

$$s(t) = \sqrt{2t}\left(1 - \frac{\epsilon}{6} + \frac{23\epsilon^2}{360}\right). \tag{168}$$

Note, this equation agrees to first order with equation (146), however we now have the second order correction. In fact there is no limit as to which order we can take the expansion, except that it becomes increasingly tedious to calculate higher order solutions. For this reason we will only work up to the second order approximation. Also, note we have already increased the order of the solution from that in §3.4.2. Now that we have solved for v_0, v_1 and v_2 we have the solution to the second order of (132) by the boundary immobilisation method,

$$u(x, t) = 1 - \frac{x}{s} + \epsilon\left[\frac{x}{6s}\left(\frac{x^2}{s^2} - 1\right)\right] + \epsilon^2\left[-\frac{x^5}{s^5 40} - \frac{x^3}{s^3 36} + \frac{x19}{s360}\right], \tag{169}$$

where $s(t)$ is given by equation (168).

3.4.4 Results

The following solutions are calculated with $\epsilon = 0.465$ ($\beta = 2.15$). Using the parameter values from Table 2, this value of ϵ suggests $\triangle T$ is approximately $2^o C$ which ensures a slow melting process.

In Fig. (6(a)) we present a comparison of the temperature at $t = 0.1$ obtained from the exact solution, equation (99), and the leading and first order perturbed solutions, (141) and (143). These are shown as solid, dashed and dotted lines respectively. As expected the first order solution is more accurate than the leading order solution. This is seen more clearly in Fig. (6(c)) which shows the absolute error as defined in (50). The maximum error for the leading order solution is approximately 7% whilst the first order has a maximum error of approximately 1%.

The position of the melt front is presented in Fig. (6(b)) with the corresponding error, defined by (129), shown in Fig. (6(d)). The leading order solution, equation (**??**), and the first order solution, equation (146), are compared to the exact solution, equation (98). The leading order is multiplied by a factor of $1 - \frac{\epsilon}{6} = 0.92$

to get the first order approximation. As the size of ϵ decreases (β increases) $1 - \frac{\epsilon}{6} \to 1$ and the leading order and first order approximations for $s(t)$ will give similar results and will approach the exact solution.

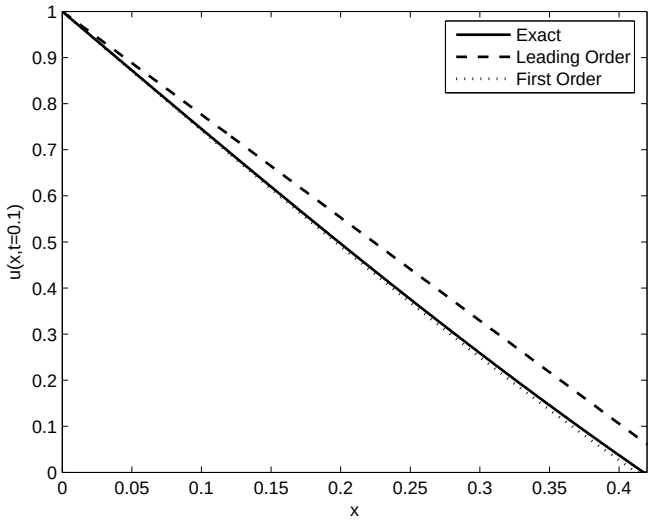

(a) Representation of the temperature profile.

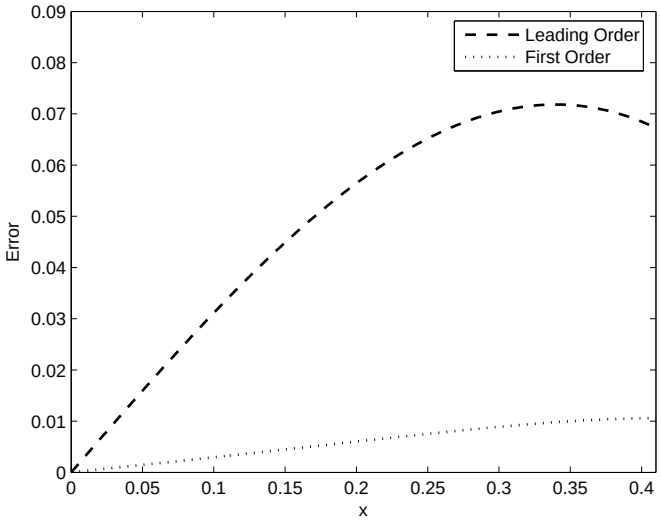

(c) Absolute error in approximating the temperature profile.

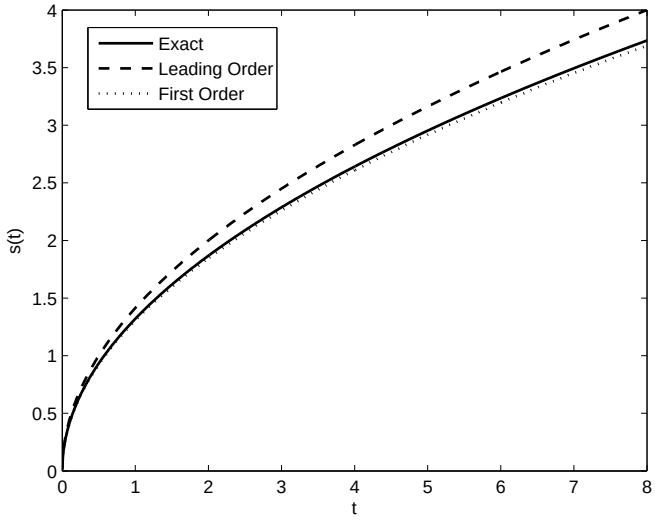

(b) Representation of the position of the melt front.

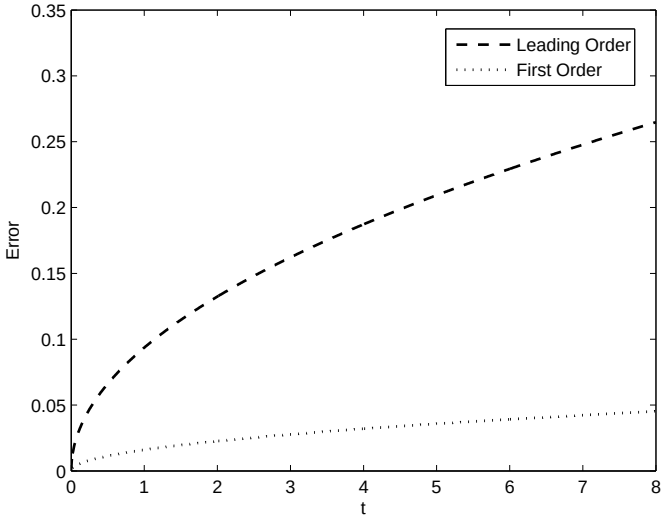

(d) Absolute error in approximating the position of the melt front.

Figure 6: Plots of the exact solution (solid line), leading order (dashed line) and first order (dotted line) of the perturbed solution.

To obtain a higher order of approximation the BIM was implemented. In Fig. (7(a)) we show the temperature profile at $t = 0.1$ obtained by the exact solution, equation (99), compared to the leading order, first order and second order BIM solutions, equations (162), (164) and (165) respectively. These are shown as solid, dashed, dot-dashed and dotted lines respectively. With the same legend key, the position of the melt front is presented in Fig. (7(b)). The absolute errors of the temperature and melt front approximations, defined by equations (50) and (129), are plotted in Figs. (7(c)) and (7(d)). A similar trend is seen; as we increase the order of approximation the error decreases. The first order solution has a maximum error of approximately 1.2%. The advantage of the higher order perturbation is evident when considering the second order solution. In fact, it is indistinguishable from the exact solution with maximum error 0.03%.

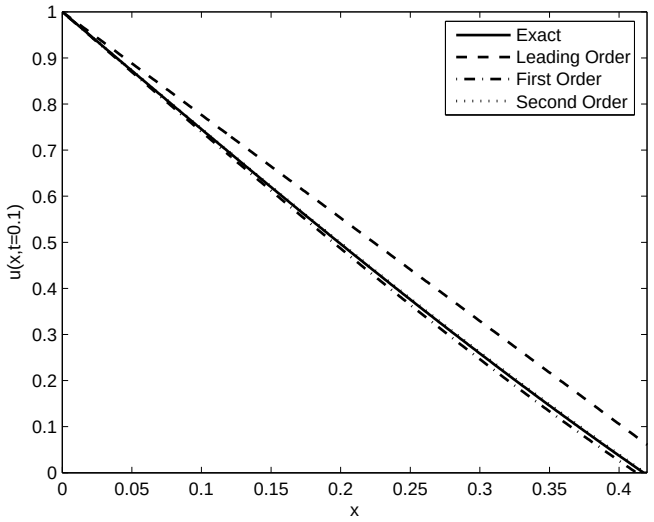

(a) Representation of the temperature profile.

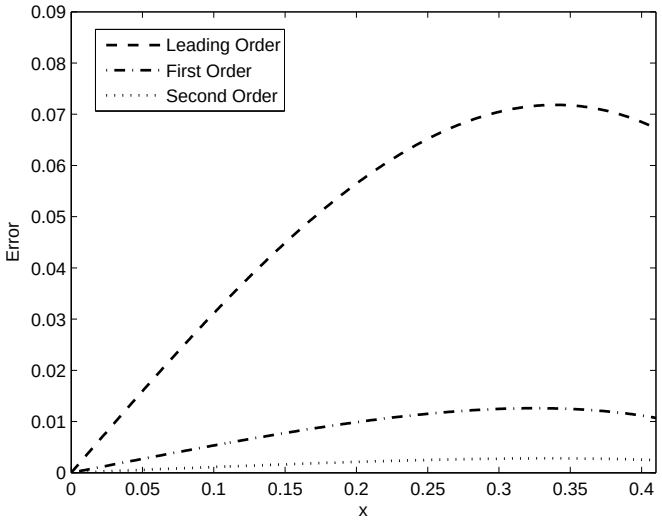

(c) Absolute error in approximating the temperature profile.

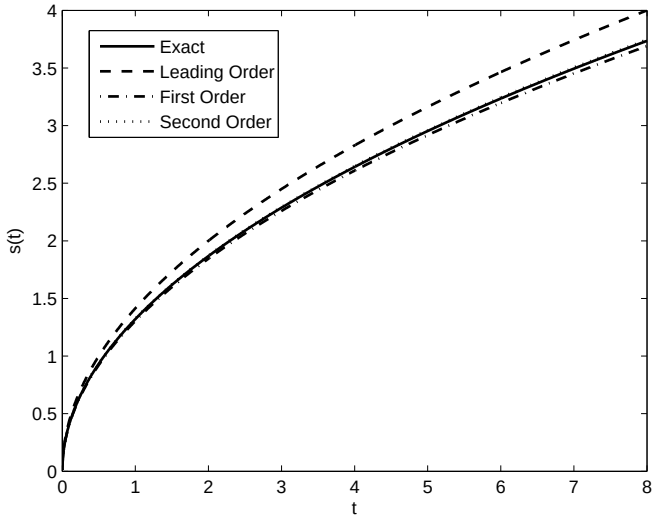

(b) Representation of the position of the melt front.

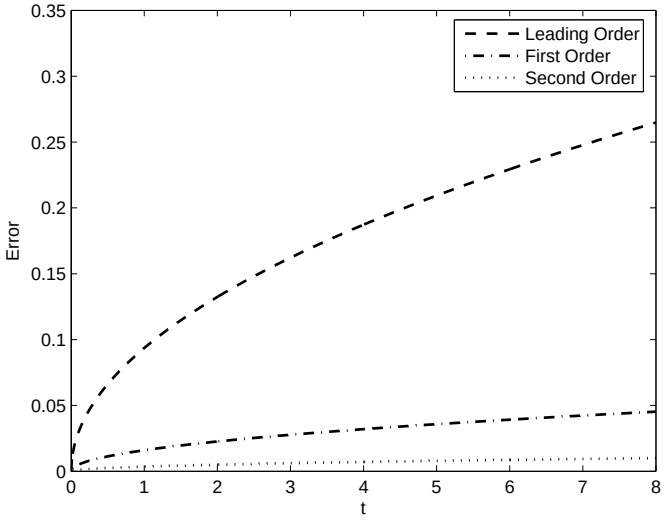

(d) Absolute error in approximating the position of the melt front.

Figure 7: Plots of the exact solution (solid line), leading order (dashed line), first order (dot-dashed line) and second order (dotted line) of the perturbed solution.

A comparison of all the methods implemented at $t = 0.1$ is shown in Figs (8(a)) and (8(b)). The errors defined by (50) are presented in Fig. (8(a)) for the first order perturbed solution, equation (143), the second order perturbed solution, equation (165), the optimal HBIM with $n = 1.765$, the optimal RIM with $n = 1.779$ and the CIM with $n = 1.524$. These are shown as dashed, dot-dashed, black dotted, blue dotted and red dotted lines respectively. With the same legend key, the errors of the melt front, as defined by (129), are shown in Fig. (8(b)). Note, in the figures the second order perturbed solution is labelled as 'BIM' in the legend and the values of n for HBIM and RIM were calculated by minimizing the error in (119) with $\beta = 2.15$. The percentage errors of the melt front predictions are shown in the table below.

Percentage errors of s(t), where $\beta = 2.15$.		
Perb. 1^{st} order		1.21%
Perb. 2^{nd} order		0.27%
HBIM	$n = 1.765$	0.85%
RIM	$n = 1.779$	0.01%
CIM	$n = 1.546$	0.07%

According to Fig. (8(a)) the second order perturbation method offers a solution with the lowest maximum error for the temperature profile, but in a Stefan problem the most important quantity is the position of the melt front so we look to Fig. (8(b)). This plot compares results of the different methods implemented and we can see that the optimal exponent RIM is best at estimating melt front with an error of approximately 0.01%. This leads us to believe that the optimal exponent RIM is the better of all the methods compared here, but before we make such a bold concluding statement we need to investigate the performance of the RIM for other β values.

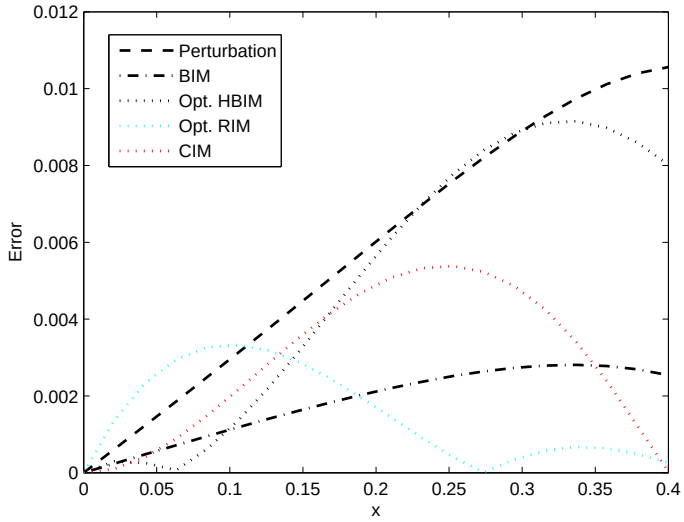

(a) Representation of the absolute error in approximating the temperature profile.

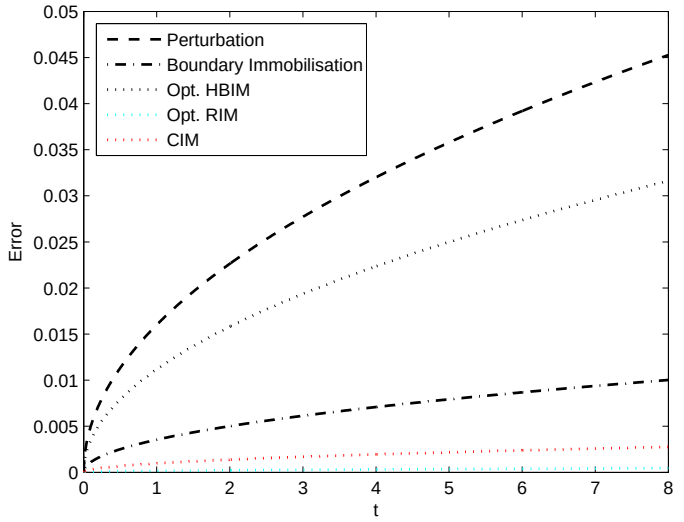

(b) Representation of the absolute error in approximating the position of the melt front.

Figure 8: Comparison of all methods: exact (solid line), 1^{st} order perturbed (dashed line), 2^{nd} order perturbed (dot-dashed line), optimal exponent HBIM (black dotted line), optimal exponent RIM (blue dotted line) and CIM (red dotted line)

Furthermore, it is clear from these figures that the 2^{nd} order perturbed solution performs better than the standard perturbation method (without a boundary immobilisation). In fact, the standard perturbation method performs poorly in comparison to all integral methods implemented. In light of this, we will compare the optimal exponent RIM to the 2^{nd} order perturbed solution for different values of β. For enrichment, we will also compare the RIM to the CIM, the next best integral method.

In Fig. (9) we have plotted the logarithm of the relative error of the optimal RIM (solid line), the 2^{nd} order perturbed solution (dashed line) and the CIM (dot-dashed line) across a large range of β-values, i.e. $\beta \in [1, 300]$. We can see the optimal RIM performs best for all values of approximately $\beta < 140$. For values of β greater than this the 2^{nd} order perturbed solution will return a lower error. We also note that the CIM is never the

best estimator, but for small values of β it is better than the 2^{nd} order perturbed solution, since it relies on the assumption $1/\beta << 1$. From this, we conclude that the choice of method depends on the value of the Stefan number in the problem. Note, β is not usually greater than 150, typical β values for water and paraffin wax are $\beta \in [1, 10]$, for metals $\beta \in [0.1, 1]$ and even smaller values for silicates [24].

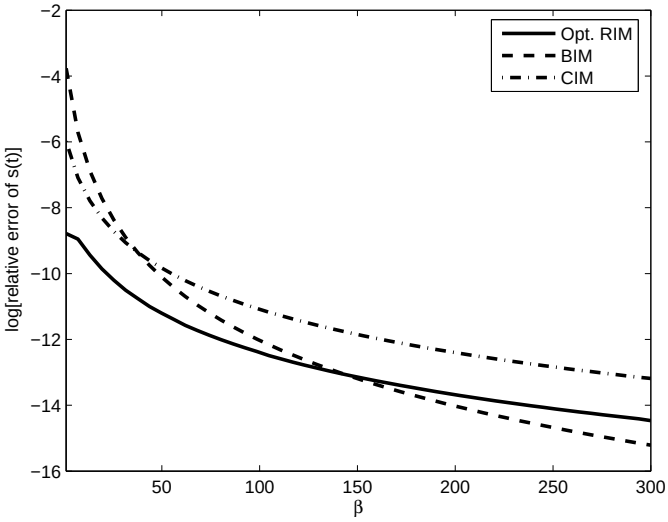

Figure 9: Comparison of the logarithm of the relative errors of the optimal RIM (solid line), 2^{nd} order perturbed solution (dashed line) and CIM (dot-dashed line).

4 Two phase Stefan problem

Now we consider the two phases of the substance (solid and liquid) and denote the temperature of the solid as θ. Initially we have a solid at a temperature above the solidus,

$$\theta(x,0) = T_\infty, \tag{170}$$

and at the boundary $x = 0$ heat is applied such that the liquid has a boundary condition,

$$T(0,t) = T_0 > T_m. \tag{171}$$

There is no initial condition for the liquid layer since there is no liquid present at $t = 0$. However, the melt front, $s(t)$, has an initial condition $s(0) = 0$ and the front is defined as the interface of the solid and liquid constituents,

$$\theta(s,t) = T(s,t) = T_m. \tag{172}$$

The temperature at the extreme of the semi-infinite plane is defined by,

$$\theta \to T_\infty \quad \text{as} \quad x \to \infty. \tag{173}$$

The two phase Stefan problem can be described by the equations,

$$T_t = \alpha_l T_{xx}, \quad 0 \le x \le s(t) \tag{174}$$

$$\theta_t = \alpha_s \theta_{xx}, \quad x \ge s(t) \tag{175}$$

with the Stefan condition given by

$$\rho_s L_m \frac{ds}{dt} = k_s \frac{\partial \theta}{\partial x}\bigg|_{x=s(t)} - k_l \frac{\partial T}{\partial x}\bigg|_{x=s(t)}, \tag{176}$$

boundary conditions (171) and (172) and the initial condition (170).

4.1 The nondimensional problem

To make the problem nondimensional we set

$$\hat{v} = \frac{\theta - T_m}{T_m - T_\infty}. \tag{177}$$

and use the same rescalings as in (85). Dropping the hats the initial and boundary conditions become

$$v(x,0) = -1, \tag{178}$$

$$i) \quad u(0,t) = 1, \quad ii) \quad u(s,t) = v(s,t) = 0, \quad iii) \quad v \to -1 \quad \text{as} \quad x \to \infty, \quad t \ge 0. \tag{179}$$

Choosing a timescale of $\tau = X^2/\alpha_l$ the governing equations (174) and (175) and the Stefan condition in (176) become,

$$u_{xx} = u_t, \quad 0 < x < s \tag{180}$$

$$\alpha v_{xx} = v_t, \quad x > s \tag{181}$$

$$\beta \frac{ds}{dt} = k \frac{\partial v}{\partial x}\bigg|_{x=s(t)} - \frac{\partial u}{\partial x}\bigg|_{x=s(t)}, \tag{182}$$

with

$$\alpha = \frac{\alpha_s}{\alpha_l}, \quad \beta = \frac{\rho_s}{\rho_l} \frac{L_m}{c_l(T_0 - T_m)}, \quad k = \frac{k_s}{k_l} \frac{T_m - T_\infty}{T_0 - T_m}. \tag{183}$$

4.2 Exact solution using similarity variables

The exact solution to the temperature in the liquid has been found in (99). The temperature profile in the solid is assumed to take a similar form to that of the liquid, so it is logical to try a profile involving the complementary error function,

$$v(x,t) = A + B\text{erfc}\left(\frac{x}{\sqrt{4t}}\right). \tag{184}$$

Applying conditions (179 ii) and (179 iii) the constants A and B are found,

$$v(x,t) = -1 + \frac{\text{erfc}\left(\frac{x}{\sqrt{4t}}\right)}{\text{erf}(\lambda)}. \tag{185}$$

The relationship in (100) is still valid here and applying the Stefan condition (176) an equation to determine λ is found,

$$\beta\lambda\sqrt{\pi} = \frac{e^{-\lambda^2}}{\text{erfc}(\lambda)} + \frac{e^{-\lambda^2}}{\text{erf}(\lambda)}. \tag{186}$$

This allows us to solve for λ numerically and thus find the moving boundary in (98) which in turn u and v can be computed. This solution will be used to check the following approximate solutions.

4.3 Approximate solutions

Although in the one phase Stefan problem we showed that the optimal RIM performed better than the optimal HBIM there is no proof that this will always be the case. In fact, for certain situations the RIM can improve on the HBIM, but there is no set rule on when it will be the best method [24]. For this reason we will apply both the optimal RIM and the optimal HBIM here.

4.3.1 Optimal heat-balance integral method

The HBIM is applied to both the solid and liquid constituents so it is standard to introduce a penetration depth, δ, which describes the moving boundary within the solid while the melt front, s, describes the position at which the phase change takes place. With the introduction of the penetration depth, the boundary condition (179 iii) is replaced with

$$v|_{x=\delta} = -1, \tag{187}$$

which reduces the problem to a finite region which is key for implementing the integral methods, and to ensure the temperature profile is smooth we impose a further condition,

$$v_x|_{x=\delta} = 0. \tag{188}$$

Both s and δ are unknowns that are determined as part of the solution process using the initial conditions $s(0) = \delta(0) = 0$. Applying the HBIM to both phases we obtain (106) for the liquid and for the solid:

$$-\alpha v_x(s,t) = \frac{d}{dt}\int_s^\delta v dx + \delta_t. \tag{189}$$

The temperature profiles for the solid and liquid components are assumed to be

$$v = a_s + b_s\left(1 - \frac{x}{\delta}\right) + c_s\left(1 - \frac{x}{\delta}\right)^m \quad \text{and} \quad u = a_l + b_l\left(1 - \frac{x}{s}\right) + c_l\left(1 - \frac{x}{s}\right)^n \tag{190}$$

respectively, where m and n is determined by minimising the function defined in (119). These were found, by Myers [16], to be $n = m = 2.233$. Applying conditions (179 i) and (179 ii) the liquid profile reduces to

$$u(x,t) = b_l\left(1 - \frac{x}{s}\right) + (1 - b_l)\left(1 - \frac{x}{s}\right)^n, \quad 0 < x < s \tag{191}$$

and applying conditions (187), (188) and (179 ii) the solid profile becomes

$$v(x,t) = -1 + \frac{(\delta - x)^m}{(\delta - s)^m}, \quad s < x < \delta. \tag{192}$$

There are only three unknowns: s, δ, and b_l. These can be solved for with the aid of the Stefan condition (182) coupled with the HBIM formulations in (106) and (189). Substituting the liquid profile (191) into (106) we obtain an expression for the melt front,

$$s(t) = 2\gamma_l\sqrt{t}, \tag{193}$$

with

$$\gamma_l = \sqrt{\frac{n(n+1)(1-b_l)}{2 + b_l(n-1)}}. \tag{194}$$

To find a simple expression for δ we substitute the temperature profiles for u and v in the Stefan condition (176) which gives

$$\beta s_t = \frac{b_l}{s} + \frac{mk}{s - \delta}, \tag{195}$$

and together with (194) we find

$$\delta(t) = 2\gamma_s\sqrt{t}, \tag{196}$$

with

$$\gamma_s = \gamma_l - \frac{m\gamma_l k}{2\beta\gamma_l^2 - b_l}. \tag{197}$$

Now $s(t)$ and $\delta(t)$ are solved for, but b_l, γ_l and γ_s are still unknown. These constants are solved using equations (194, 197) and to close the system a third relation is required. This is found by substituting the solid profile (192) and the expressions for γ_l and γ_s into the HBIM formulation (189). The time dependence drops out leaving a simple relation,

$$\frac{\alpha m(m+1)}{2(\gamma_s - \gamma_l)} = m\gamma_l + \gamma_s. \tag{198}$$

So in order to solve this 2 phase problem we use equations (194), (197), (198) to find b_l, γ_l and γ_s. Then we use these values to calculate $s(t)$ and $\delta(t)$ via equations (193), (196) and substituting in equations (191), (192) we obtain the temperature profiles.

4.3.2 Optimal refined integral method

A similar analysis is followed as in section §4.3.1, but now a double integration is carried out on the heat equations. For the liquid constituent we integrate the heat equation (180) twice to give,

$$\frac{d}{dt}\int_0^s xu dx = u|_{x=0} + s\left.\frac{\partial u}{\partial x}\right|_{x=s} \tag{199}$$

Previously, the Stefan condition was substituted in place of the $u_x(s,t)$ term to increase the accuracy, but now the Stefan condition contains the term $v_x(s,t)$ which only makes calculations more complicated. So instead we will substitute the temperature profile for $u_x(s,t)$.

For the solid constituent, with dummy variable y replacing x, a double integration over the heat equation gives,

$$\int_s^\delta \int_x^\delta \frac{\partial v}{\partial t} dy dx = \int_s^\delta \int_x^\delta \alpha \frac{\partial^2 v}{\partial x^2} dy dx. \tag{200}$$

The right hand side can be evaluated with the use of conditions $v(\delta) = -1$ and $v(s) = 0$ we get,

$$\int_s^\delta \int_x^\delta \alpha \frac{\partial^2 v}{\partial x^2} dy dx = \alpha \int_s^\delta \left[\left. \frac{\partial v}{\partial x} \right|_{x=\delta} - \left. \frac{\partial v}{\partial x} \right|_x \right] dx = \alpha \left[x v_x(\delta) - v(x,t) \right] \Big|_s^\delta = \alpha. \tag{201}$$

The left hand side can be integrated by parts [6],

$$\int_s^\delta \int_x^\delta \frac{\partial v}{\partial t} dy dx = \left[x \int_x^\delta \frac{\partial v}{\partial t} dy \right] \Big|_s^\delta + \int_s^\delta x \frac{\partial v}{\partial t} dx, \tag{202}$$

$$= -s \int_s^\delta \frac{\partial v}{\partial t} dx + \int_s^\delta x \frac{\partial v}{\partial t} dx. \tag{203}$$

Using the Leibniz integration rule we obtain,

$$\int_s^\delta \int_x^\delta \frac{\partial v}{\partial t} dy dx = -s \frac{\partial}{\partial t} \int_s^\delta v dx - s\delta_t + \int_s^\delta x \frac{\partial v}{\partial t} dx. \tag{204}$$

Now equating (201) with (204) and applying the heat balance integral (189) we obtain the refined integral for the solid constituent,

$$\frac{d}{dt} \int_s^\delta x v dx + \delta \frac{d\delta}{dt} = \alpha \left(1 - s \left. \frac{\partial v}{\partial x} \right|_{x=s} \right). \tag{205}$$

The temperature profiles are the same as that in the HBIM, given by the expressions (191) and (192), where $n = m = 2.219$ [16]. Following the same procedure as that in the previous section we find 3 relations in order to solve for the three unknowns: s, δ, and b_l.

Applying the liquid temperature profile (191) to the refined integral (199) we obtain an expression for the melt front,

$$s(t) = 2\gamma_l \sqrt{t}, \tag{206}$$

with

$$\gamma_l = \sqrt{\frac{6(1-b_l)(n+1)(n+2)}{4(-4b_l + b_l n^2 + 3b_l n + 6)}}. \tag{207}$$

Since we are using the same temperature profiles for u and v (equations (191), (192)) as the HBIM, when applying them to the Stefan condition (182) we find the expression for $\delta(t)$ is given by (196) with γ_s defined as in (197). As we have expressions for $s(t)$ and $\delta(t)$ the three unknowns are now: b_l, γ_l and γ_s. These are solved for with equations (194) and (197). To close the system the final equation comes from applying the solid profile and the expressions for γ_l and γ_s to the refined integral (205),

$$\gamma_l^2 m(m+1) + 2\gamma_l \gamma_s m + 2\gamma_s^2 = \frac{\alpha(m+1)(m+2)}{2} \left(1 - \frac{m\gamma_l}{\gamma_l - \gamma_s} \right). \tag{208}$$

[6] From the second fundamental theorem of calculus we can calculate $\frac{\partial}{\partial x} \left[\int_x^\delta \frac{\partial v}{\partial t} dy \right] = -\frac{\partial}{\partial x} \left[\int_\delta^x \frac{\partial v}{\partial t} dy \right] = -\frac{\partial v(x,t)}{\partial t}$

4.3.3 Results

For simplicity we assume the thermal properties remain the same through the phase change (i.e. densities are constant in time, etc). In the reported results we assume $\alpha = k = 1$, since when working with a phase transition, for example between water and ice, the density difference between the materials is not extreme.

Furthermore, constants b_l, γ_l and γ_s are solved for using Matlab's $fsolve$ function which finds a zero of the system of equations (194,197,198) for the HBIM and equations (197,207,208) for the RIM.

In Fig. 10(a) the temperature profiles of the solid and liquid constituents by the optimal HBIM with $n = m = 2.235$ (dashed line) and the optimal RIM with $n = m = 2.219$ (dotted line) are plotted against the exact solution (solid line). The stars on the plot represent the liquid height and the heat penetration depth of the HBIM, while the stars are those estimated by the RIM. The temperature profile that lies above 0 is that of the liquid and below is the solid profile.

In Fig. 10(b) the position of the melt fronts predicted by the HBIM (dashed line) and RIM (dotted line) are compared to the exact (solid line) with the error defined by (129). The error plot takes on the same shape as the progression of the melt front suggesting the error does not change with time. The relative error of the predicted melt front is 4.8% for the HBIM and 2.6% for the RIM.

Now that we understand approximate methods for calculating temperature we will apply our knowledge to contact melting. Since the optimal HBIM is easy to implement and offers a relatively accurate approximation we will use this method in the following section that deals with contact melting.

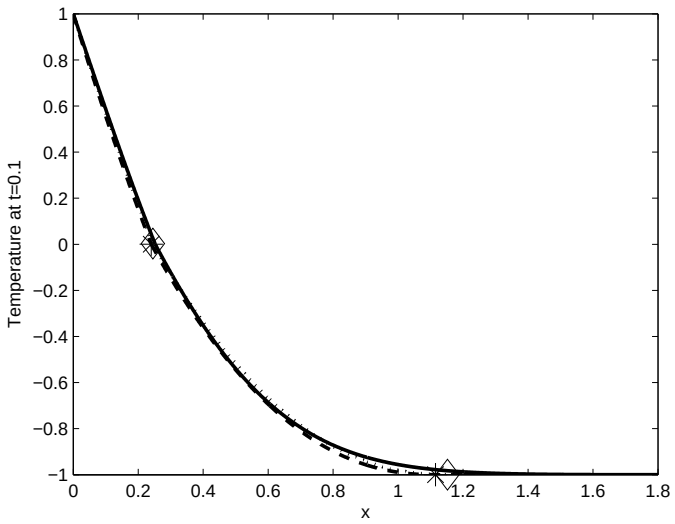

(a) Representation of the temperature profile at $t = 0.1$.

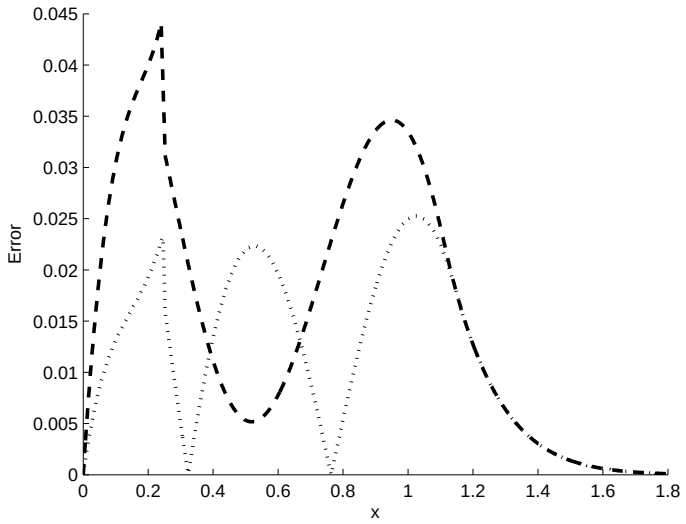

(c) Absolute error in the approximating the exact solution at $t = 0.1$.

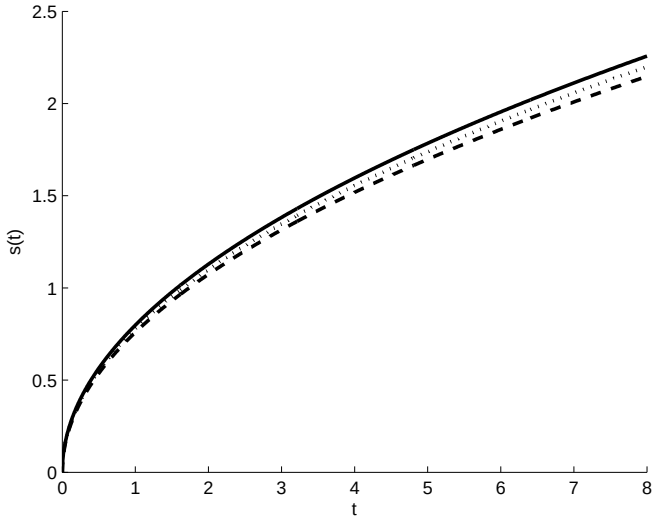

(b) Representation of the position of the melt front.

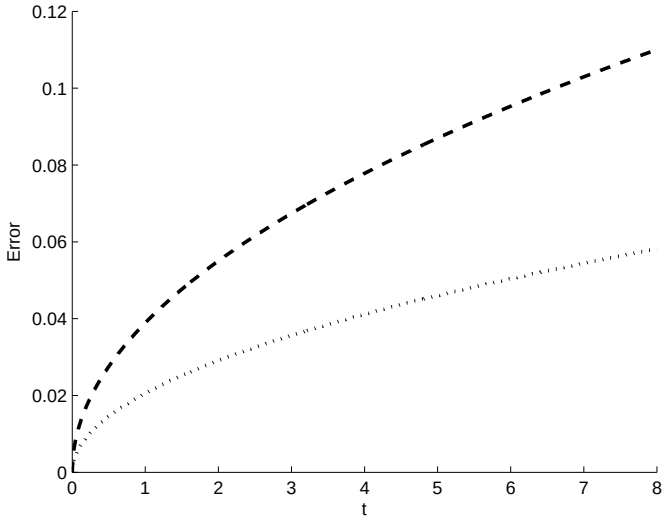

(d) Absolute error in approximating the position of the melt front.

Figure 10: Plots of the exact solution (solid line), optimal HBIM with $n = m = 2.235$ (dashed line) and the optimal RIM with $n = m = 2.219$ (dotted line).

5 3D contact melting

5.1 Introduction

Contact melting is a process where a phase change material (PCM), initially at θ_0, comes into contact with a surface that is at a temperature T_0 which is above the phase change temperature of the PCM, T_m. As a result of this the PCM begins to melt and a liquid layer is formed. The weight of the PCM that is still in solid form pushes down on the liquid. This forces the liquid out from under the solid and so the liquid layer remains thin.

In line with the experiments of Moallemi [13] we model a PCM that is cuboid and placed on a flat surface. The top and sides are insulated. Then we may split the melting process into 3 stages. The first stage is the pre-melt stage, which occurs from the time the cuboid comes into contact with the heated surface until the block reaches melting temperature, T_m, and melting begins. So the first stage is very short and occurs for $t \in [0, t_1]$ where t_1 is determined by settling $\theta|_{z=0} = T_m$. The second stage is the stage in which the liquid layer is formed and the block begins to float upon it. This stage occurs for $t \in [t_1, t_2]$ and ends when the temperature at the top of the solid rises above the initial θ_0. So t_2 is the time at which $\theta|_{z=H+h} > \theta_0$ occurs. Finally, stage 3 begins at t_2 and ends once all the block is melted, i.e. $t \in [t_2, t_m]$.

The modelling process requires the calculation of the temperature gradients in both the liquid and solid constituents as well as the pressure gradient and flow velocity of the liquid. This process has been modelled in 2 dimensions by Myers, Mitchell and Muchatibaya [19], who also highlighted the extension to the 3 dimensional model which we wish to improve upon. We will use the techniques discussed in the previous sections to solve the problem. We will do the initial analysis using parameter values of water and ice. Finally, we will apply the method to n-octadecane and validate our results by comparing them with experimental data provided by Moallemi. The results from this section have been written in to a paper, with co-author Tim Myers, and has been submitted for publishing.

5.2 Problem description

A block of PCM initially at a temperature of θ_0 is placed on a heated surface. The block has the dimensions of $2L \times 2W \times H$, so the width is described along $x \in [-L, L]$, the breadth $y \in [-W, W]$ and the height $z \in [0, H]$. To focus solely on the heating of the solid from the substrate we will prescribe boundary conditions to ensure an insulated block.

The height of the liquid layer is denoted as $h(t)$, occupying $z \in [0, h]$, and the melted solid as $h_m(t)$. Initially the solid has a height of $H(0) = H_0$ and as melting occurs $H(t) = H_0 - h_m(t)$. The liquid is squeezed out at the sides of the block by the pressure exerted by the remaining mass of the solid, $M = 4\rho_s LW[H_0 - h_m]$.

Since the block is insulated the heat transfer is one-dimensional. So in this model we make the general 1D heat equation assumptions as specified in §2.1, but now the heat flow will be in the $z-$direction. In addition to that we assume that the lubrication approximation holds in the liquid layer. So the flow in the liquid film remains laminar (parallel to the solid surface) and it is driven by the pressure gradient. In the past, other mathematicians have made use of some assumptions that we will not. These include:

1. The temperature of the solid remains at the melting temperature, T_m, throughout the process.
2. The melting process is in a quasi-steady state, that is, at every point in time the weight of the solid is balanced by the excess pressure built in the liquid film. So if the position of the melt front is denoted $h(t)$ then $h_t = 0$. A model using this assumption is referred to as a 'quasi-steady' model.
3. The amount of melted fluid is small compared to that of the initial solid.

4. There is a perfect thermal contact between the liquid and the substrate or there is a constant flux.

5. The model is 2D.

See [19], [11], [10]. Assumption (1) may be overcome by applying the optimal exponent HBIM to the solid in each of the 3 melting stages. Assumption (2) may be avoided by introducing a force balance equation that will solve for the unknown liquid height, $h(t)$. Assumptions (3) and (4) are omitted as we allow the solid to decrease in mass with time and we apply a Newton cooling condition (see equations (238) and (240)). And finally, assumption (5) is ignored as we have a 3D model.

5.3 Governing equations

As in the two phase Stefan problem the temperature gradient in both the liquid and solid is calculated. In addition to this, we need to determine the flow of the liquid layer between the surface and the solid block. So it is necessary to determine the velocity field and the pressure gradient within the liquid. For this we assume the liquid layer to be sufficiently small in comparison to the height of the solid and a laminar flow regime in the thin layer so Navier-Stokes equations are used with a lubrication approximation. Using the appropriate scalings we can write the well known non-dimensional equations:

$$\begin{aligned} \eta \tfrac{\partial^2 \mathsf{u}}{\partial z^2} &= \tfrac{\partial p}{\partial x}, \\ \eta \tfrac{\partial^2 \mathsf{v}}{\partial z^2} &= \tfrac{\partial p}{\partial y}, \\ \tfrac{\partial p}{\partial z} &= 0, \end{aligned} \tag{209}$$

where η is the viscosity, the velocity vector is given by $\vec{u} = (\mathsf{u}, \mathsf{v}, \mathsf{w})$ for the x-, y- and z-directions respectively and p is the pressure. In this rescaling the largest term that has been neglected is $\mathcal{O}(\epsilon^2 Re)$ where, if H were the height scale and L the length scale, $\epsilon^2 Re$ is the reduced Reynolds number and $\epsilon = H/L$ [19]. The Reynolds number, Re, expresses the ratio of inertial (resistant to change or motion) forces to viscous forces (force arising from viscous effects). Since viscous forces are dominant the flow is laminar which suggests a small Reynolds number. Also, the length scale is much greater than that of the height scale so $\epsilon \ll 1$ and so $\epsilon^2 Re \ll 1$, verifying that the largest neglected term is in fact small. The flow is incompressible so the continuity equation reads as

$$\frac{\partial \mathsf{u}}{\partial x} + \frac{\partial \mathsf{v}}{\partial y} + \frac{\partial \mathsf{w}}{\partial z} = 0. \tag{210}$$

This states that the incoming flux matches the outgoing flux exactly and so there are no sources or sinks in the system. We prescribe the standard no slip conditions at $z = 0$,

$$\mathsf{u}(0) = \mathsf{v}(0) = \mathsf{w}(0) = 0, \tag{211}$$

and at the top of the liquid layer there is no slip in the x- and y-direction,

$$\mathsf{u}(h) = \mathsf{v}(h) = 0. \tag{212}$$

The final condition required to solve the flow equations is derived from a momentum balance in the z-direction:

$$\rho_s \vec{n} \cdot (\vec{u_s} - \vec{u_b}) = \rho_l \vec{n} \cdot (\vec{u_l} - \vec{u_b}), \tag{213}$$

where $\vec{u_s}$, $\vec{u_l}$ and $\vec{u_b}$ are the velocity vectors in the solid, liquid and boundary respectively and $\vec{n}$ is the normal vector at the solid-liquid interface. In our case these are

$$\vec{n} = (0, 0, 1), \quad \vec{u_s} = (0, 0, h_t - h_{mt}), \quad \vec{u_l} = (\mathsf{u}, \mathsf{v}, \mathsf{w}) \quad \vec{u_b} = (0, 0, h_t). \tag{214}$$

Substituting these vectors into the momentum balance equation and rearranging them we can define the $z-$directional velocity of the fluid at $z = h$ as,

$$\mathsf{w}(h) = \frac{\partial h}{\partial t} - \frac{\rho_s}{\rho_l}\frac{\partial h_m}{\partial t}. \tag{215}$$

To relate the pressure to the height of the liquid layer, h, a force balance equation, is introduced:

$$Mg - pA = M\frac{d\mathsf{W}}{dt}, \tag{216}$$

where $\mathsf{W} = \frac{dh}{dt} - \frac{dh_m}{dt}$ is the vertical velocity of the solid and A is the area of contact between the solid block and liquid layer and gravity is denoted by g. Here the acceleration term, $\frac{d\mathsf{W}}{dt}$, is neglected as acceleration due to gravity is dominant. For more detail see [19]. With the mass of the block given by $M = 4\rho_s LW[H_0 - h_m(t)]$ the force balance becomes,

$$4\rho_s LW[H_0 - h_m(t)]g = \int_{-L}^{L}\int_{-W}^{W} p dy dx, \tag{217}$$

where the breadth of the block is 2L and the width 2W. This equation describes the balance between the weight of the solid and the pressure exerted by the liquid to support that weight.

The liquid velocities in the $x-$ and $y-$directions can be calculated from equation (209). With the conditions as described in (211) and (212) the velocities are found in terms of the pressure gradient,

$$\mathsf{u} = \frac{p_x}{2\eta}z(z-h), \quad \mathsf{v} = \frac{p_y}{2\eta}z(z-h). \tag{218}$$

An equation for the pressure gradient is found by integrating the incompressibility condition (210) across the height of the liquid layer $z \in [0, h]$,

$$\frac{d}{dz}\int_0^h \mathsf{w}dz = -\frac{d}{dx}\int_0^h \mathsf{u}dz - \frac{d}{dy}\int_0^h \mathsf{v}dz. \tag{219}$$

Substituting (218) and (215) into the above expression we obtain,

$$\mathsf{w}(h) - \mathsf{w}(0) = \frac{h^3}{12\eta}\nabla^2 p \tag{220}$$

$$\frac{\partial h}{\partial t} - \frac{\rho_s}{\rho_l}\frac{\partial h_m}{\partial t} = \frac{h^3}{12\eta}\nabla^2 p \tag{221}$$

Rearranging this we obtain a form of Poisson's equation that governs the pressure distribution,

$$\nabla^2 p = \frac{12\eta}{h^3}\left(\frac{\partial h}{\partial t} - \frac{\rho_s}{\rho_l}\frac{\partial h_m}{\partial t}\right) = f(t), \tag{222}$$

with boundary conditions stipulating ambient pressure outside the block,

$$p(\pm L, y) = p(x, \pm W) = 0. \tag{223}$$

With the substitution of the eigenfunction expansion,

$$p = \sum_{n=1}^{\infty} b_n(s)\sin(\omega_n r) \tag{224}$$

and a shift of axes,

$$r = \frac{x+L}{2}, \quad s = \frac{y+W}{2}, \tag{225}$$

equation (222) becomes

$$\sum_{n=1}^{\infty}\left(\frac{\partial^2 b_n}{\partial s^2}-\omega^2 b_n\right)\sin(\omega_n r)=4f(t), \tag{226}$$

where $\omega_n = n\pi/L$. By orthogonality of the sine function the expression in brackets can be written as

$$\begin{aligned}\frac{\partial^2 b_n}{\partial s^2}-\omega^2 b_n &= 4f(t)\frac{2}{L}\int_0^L \sin(\omega_n\theta)d\theta &(227)\\ &= 8f(t)\frac{1-(-1)^n}{n\pi} &(228)\\ &= q_n(t). &(229)\end{aligned}$$

Considering the boundary conditions in (223) we obtain the relevant conditions to solve the above equation:

$$b_n(0)=b_n(W)=0. \tag{230}$$

Using Maple^{TM} computing software we find an expression for b_n which in turn gives the eigenfunction expansion for the pressure:

$$b_n=\frac{q}{\omega^2}\left[\frac{e^{-\omega s}(e^{\omega W}-1)}{e^{\omega W}-e^{-\omega W}}+\frac{e^{\omega s}(e^{-\omega W}-1)}{e^{-\omega W}-e^{\omega W}}\right]. \tag{231}$$

The expression for the coefficients b_n is different to that found in Myers *et al.* 3D extension in [19]. The formulation in [19] produced a flat pressure distribution. This change to the eigenfunction expansion produces a realistic distribution. Substituting the expression for pressure into the force balance equation (217) we obtain,

$$4\rho_s LW[H_0-h_m(t)]g=f\Phi, \tag{232}$$

where,

$$\Phi=\sum_{n=1}^{\infty}\frac{32(1-(-1)^n)(-2e^{\omega W}+\omega We^{\omega W}+2+\omega W)}{n\pi\omega^4(e^{\omega W}+1)}(\cos\omega L-1). \tag{233}$$

Substituting $f(t)$ from equation (222) and rearranging (232) we obtain an equation to determine the liquid height, h,

$$\frac{\partial h}{\partial t}=\frac{h^3}{12\eta\phi}4\rho_s LW[H_0-h_m]+\frac{\rho_s}{\rho_l}\frac{\partial h_m}{\partial t}. \tag{234}$$

Apart from the liquid height, pressure and velocity fields, it is also required to determine the temperature gradients in the solid and liquid. This is given by the heat equations

$$\begin{aligned}T_{xx}&=0, &(235)\\ \theta_t&=\alpha_s\theta_{xx}, &(236)\end{aligned}$$

Note we assume that the heat transfer in the liquid layer is dominated by conduction since the layer is thin. A Stefan condition will be used to determine the height of the melted solid, h_m,

$$\rho_s L_m\frac{dh_m}{dt}=k_s\left.\frac{\partial\theta}{\partial z}\right|_{z=h}-k_l\left.\frac{\partial T}{\partial z}\right|_{z=h}. \tag{237}$$

The analysis of how this provides an equation to determine the height of the melted solid will follow in §5.4.

Further boundary conditions are prescribed depending on which stage the melting process is in. During stage 1 there is no melting so with the absence of liquid only conditions for the solid are needed. A cooling condition is prescribed at $z=0$,

$$\left.\frac{\partial\theta}{\partial z}\right|_{z=0}=\frac{-q+h_{ss}(\theta-T_0)}{k_s}, \tag{238}$$

where T_0 is the substrate temperature and h_{ss} is the heat transfer coefficient between the substrate and the solid. We assume the block is insulated at $z = h + H$, i.e. there is no flux on the upper boundary,

$$\left.\frac{\partial\theta}{\partial z}\right|_{z=h+H} = 0. \tag{239}$$

Note that if we have a large heat transfer coefficient, $h_{ss} \to \infty$, it is equivalent to dealing with a fixed temperature boundary condition. If we allow $h_{ss} \to 0$ then we are dealing with a constant flux situation of $\theta_z = -q/k_s$ at $z = 0$. And since the flux will be infinite melting will occur immediately. Similarly, with h_{sl}, the heat transfer coefficient between the substrate and liquid, in the next stage. This allows us to use the same model to explore a wide range of possible scenarios with different heat fluxes. Stage 2 begins as liquid appears on the surface at $z = 0$ and boundary conditions are prescribed for the liquid. First, the cooling condition at $z = 0$ is applied to the liquid,

$$\left.\frac{\partial T}{\partial z}\right|_{z=0} = \frac{-q + h_{sl}(T - T_0)}{k_l}, \tag{240}$$

and second, a further condition is required to ensure that the melt interface remains at the melting temperature,

$$T = \theta = T_m, \quad \text{at} \quad z = h. \tag{241}$$

5.4 Analysis

The temperature profile in the liquid and solid will be calculated using the optimal exponent HBIM. We have seen in previous sections that other integral methods can offer solutions with lower error, but the error incurred by implementing the HBIM is not very high. Since this method is easy to implement and has a low error we will implement it here. The melting process is split into three stages according to the temperature distribution in the solid, so the temperature profile in the solid will be estimated for each stage.

Stage 1

During the pre-melt stage it is only necessary to approximate the solid temperature profile. At the boundary $z = 0$ we impose the cooling condition (238). With this Newton cooling scenario, following Myers [17], we assume a temperature profile of the form

$$\theta(z,t) = a + b\left(1 - \frac{z}{\delta}\right) + c\left(1 - \frac{z}{\delta}\right)^m, \tag{242}$$

where $m = 3.584$. A further two conditions come from the fact that the temperature of the solid at the heat penetration depth is negligibly different from the initial temperature, $\theta(\delta, t) = \theta_0$, and we require a smooth temperature profile, $\theta_z(\delta, t) = 0$. With these conditions we find

$$\theta(z,t) = \theta_0 + \frac{\delta(q + h_{ss}(T_0 - \theta_0))}{mk_s + \delta h_{ss}}\left(1 - \frac{z}{\delta}\right)^m. \tag{243}$$

We solve for δ by applying the HBIM: integrating the heat equation (236) over the region $z \in [0, \delta]$ and substituting the profile (243) we find a differential equation,

$$\frac{d}{dt}\left(\frac{\delta^2(q + h_{ss}(T_0 - \theta_0))}{(1+m)(mk_s + \delta h_{ss})}\right) = \frac{\alpha_s m(q + h_{ss}(T_0 - \theta_0))}{mk_s + \delta h_{ss}}, \tag{244}$$

that has an initial condition $\delta(0) = 0$. With some manipulation we find a separable equation that has an implicit solution for δ,

$$t = \frac{1}{\alpha_s m(m+1)}\left[\delta^2 + \frac{\delta^2}{2h_{ss}} - \frac{\delta m k_s}{h_{ss}^2} + \frac{mk_s}{h_{ss}^3}\ln\left(\frac{mk_s + \delta h_{ss}}{mk_s}\right)\right] \tag{245}$$

The start of melting at $z = 0$ defines the end of the first stage, i.e. t_1 is defined such that $\theta(0, t_1) = T_m$. We denote the heat penetration depth corresponding to t_1 as δ_1, which is found using equation (243),

$$\delta_1 = \frac{mk_s(T_m - \theta_0)}{q + h_{ss}(T_0 - T_m)}. \tag{246}$$

We find, using the parameter values in Table 2, that $t_1 = 3 \times 10^{-5}$s and $\delta_1 = 5.1$mm.

Stage 2

Once the melting starts we apply the HBIM to solid phase and we solve for the temperature in the liquid by integrating equation (235). Applying the cooling condition (240) and condition (241), the liquid temperature profile is found to be

$$T(z, t) = T_m - \frac{q + h_{sl}(T_0 - T_m)}{k_l + hh_{sl}}(z - h). \tag{247}$$

With the layer of water between the solid and substrate, the thermal problem in the solid has fixed temperature boundary conditions. Namely, $\theta(h) = T_m$, $\theta(\delta) = \theta_0$ and $\theta_z(\delta) = 0$. The optimal exponent for this scenario is $n = 2.235$ [17]. These conditions lead to a temperature profile of the form

$$\theta(z, t) = \theta_0 + \frac{T_m - \theta_0}{\left(1 - \frac{h}{\delta}\right)^n}\left(1 - \frac{z}{\delta}\right)^n. \tag{248}$$

Integrating the heat equation across the solid, $z \in [h, \delta]$ an equation to determine δ is found,

$$nh_t + \delta_t = \frac{\alpha_s n(n + 1)}{\delta - h}. \tag{249}$$

Finally, to find an equation to determine height of the melted solid, h_m, we substitute equations (247) and (248) into the Stefan condition (237),

$$\rho_s L_m \frac{\partial h_m}{\partial t} = \frac{k_s n(\theta_0 - T_m)}{\delta - h} + \frac{k_l(q + h_{sl}(T_0 - T_m))}{k_l + hh_{sl}}. \tag{250}$$

There are three unknowns in stage 2: δ, h and h_m with initial conditions $\delta(t_1) = \delta_1$ and $h(t_1) = h_m(t_1) = 0$. These are solved using the two equations provided by (249) and (250), while the third equation comes from the force balance described in (232).

Once the heat has penetrated through the entire solid, i.e. $\delta = h + H$, stage 3 begins. We will denote this time as t_2 and the initial conditions for stage 3 as δ_2, h_2 and h_{m2}. We find that $t_2 = 110.5$s, $\delta_2 = 0.04$mm, $h_2 = 0.00009$mm and $h_{m2} = 0.007$mm.

Stage 3

The entire solid has a temperature above the initial θ_0 so as a result we cannot impose the boundary condition $\theta(\delta) = \theta_0$. Instead, we use the fact that the block is insulated at the top, i.e. $\theta_z(H + h) = 0$. The second condition is $\theta(h) = T_m$. The temperature profile is assumed to be

$$\theta(z, t) = a + b\left(1 - \frac{z}{h + H}\right) + c\left(1 - \frac{z}{h + H}\right)^n. \tag{251}$$

Applying the conditions we solve for unknowns b and c, leaving only one unknown in the temperature profile, i.e. a instead of δ as in the previous stage:

$$\theta(z, t) = a + \frac{T_m - a}{\left(1 - \frac{h}{h+H}\right)^n}\left(1 - \frac{z}{h + H}\right)^n. \tag{252}$$

Previously we integrated the heat equation to find an equation for the final unknown parameter in the temperature profile and used an initial condition, in this case it is $a(t_2) = \theta_0$. The initial condition of a comes from the fact that we require continuity of temperature, i.e. $\theta(H + h) = \theta_0$ at $t = t_2$.

Proceeding in this way we find a complicated equation to solve for a. To simply this type of problem Goodman [9] proposed a function, ϕ, defined as the integral of the temperature over the domain of interest,

$$\phi = \int_h^{h+H} \theta dz = \frac{H}{4}(T_m + 3a). \tag{253}$$

Integrating the heat equation over the solid $z \in [h, h + H]$ leads to an equation to determine ϕ:

$$\frac{d\phi}{dt} = \frac{3k_s(T_m - a)}{H_0 - h_m} + a\left(\frac{dh}{dt} - \frac{dh_m}{dt}\right) - T_m\frac{dh}{dt}, \tag{254}$$

where a comes from (253):

$$a = \frac{1}{3}\left(\frac{4\phi}{H} - T_m\right). \tag{255}$$

Substituting the solid profile (252) and the liquid profile (247) into the Stefan condition provides an equation to determine the height of the melted solid:

$$\rho_s L_m \frac{\partial h_m}{\partial t} = \frac{-nk_s(T_m - a)}{H} + \frac{k_l(q + h_{sl}(T_0 - T_m))}{k_l + hh_{sl}}. \tag{256}$$

Again, to close the system, the force balance equation (232) provides the final equation to solve for the liquid height. The three unknowns in stage 3 are ϕ, h and h_m that have initial conditions

$$\phi(t_2) = (H_0 - h_{m2})(T_m + 3\theta_0)/4, \quad h(t_2) = h_2, \quad h_m = h_{m2}. \tag{257}$$

5.5 Results

For the first stage of the melting process the 3D model may be compared to that of the exact solution, given by:

$$\begin{aligned}\theta(z,t) = \quad & \theta_0 + \frac{q - h_{ss}(\theta_0 - T_0)}{h_{ss}}\left[\operatorname{erfc}\left(\frac{z}{\sqrt{4\alpha_s t}}\right)\right. \\ & \left. -exp\left(\frac{h_{ss}z}{k_s} + \alpha_s t\left(\frac{h_{ss}}{k_s}\right)^2\right)\operatorname{erfc}\left(\frac{z}{\sqrt{4\alpha_s t}} + \frac{h_{ss}\sqrt{\alpha_s t}}{k_s}\right)\right].\end{aligned} \tag{258}$$

The derivation of the exact solution is not reported here, but it can be determined with the use of Laplace transforms, see [18].

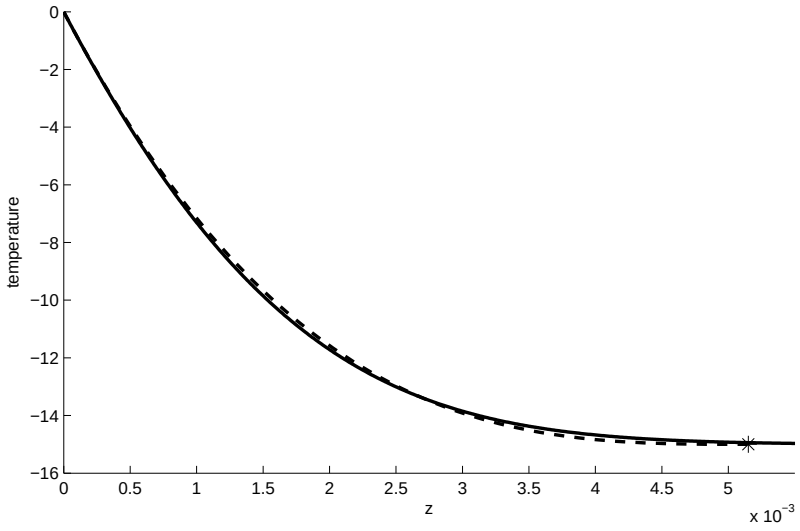

Figure 11: *The temperature in the solid at* $t_1 = 0.00003s$ *(at the end of stage 1). The solution from* (243) *(dashed line) is compared to the exact solution (solid line), where the star is the penetration depth,* $\delta_1 = 5.1mm$.

Using values from Table 2 we see in Fig. 11 the exact solution (solid line) of the temperature in the solid is compared to equation (243) (dashed line) at $t_1 = 0.00003$s. The black star indicates the penetration depth of the 3D model, $\delta_1 = 5.1$mm.

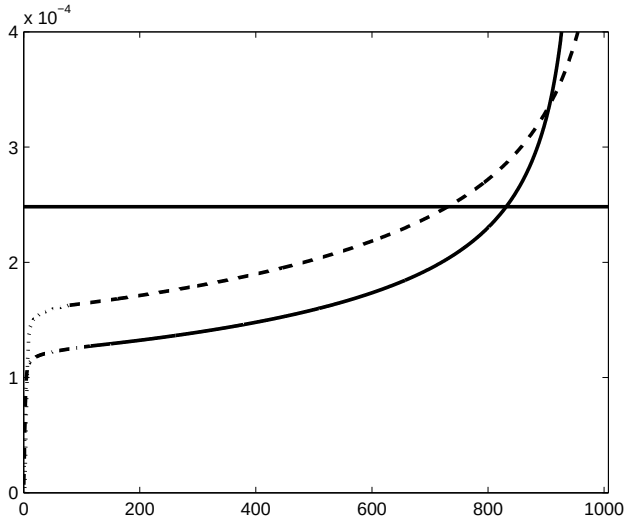

(a) $h(t)$ calculated from (234) ($t < t_2$ dot-dashed line, $t > t_2$ solid line) and by Myers's 2D model ($t < t_2$ dotted line, $t > t_2$ dashed line)

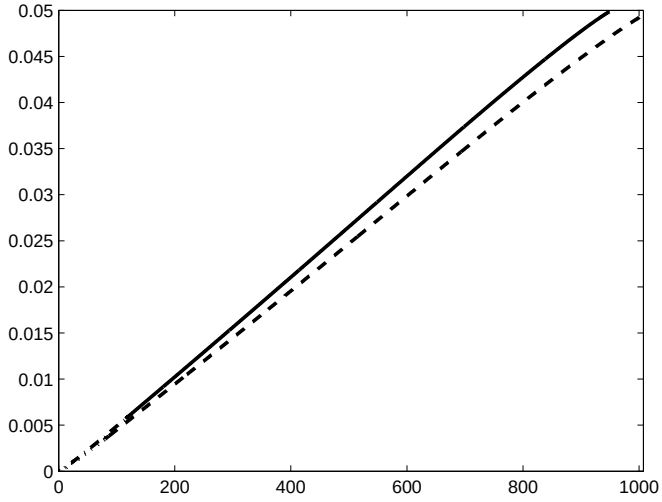

(b) $h_m(t)$ from equations (250) and (256) ($t < t_2$ dot-dashed line, $t > t_2$ solid line) and Myers's 2D model ($t < t_2$ dotted line, $t > t_2$ dashed line)

Figure 12: The liquid height is presented in (a) and the melt height in (b).

In Fig. 12(a) the height of the liquid layer is plotted for both stages 2 and 3. The height predicted by the 3D model which uses the optimal HBIM is compared with [19] which uses a cubic HBIM and assumes a 2D model. Also presented here is that of the quasi-steady model, calculated from equation (18) in [19], which assumes $h_t = 0$ is plotted as a horizontal dashed line. The height by the 3D model during stage 2 ($t_1 < t < t_2$) and stage 3 ($t > t_2$) is plotted with dot-dashed and solid lines, respectively. The height predicted by the Myers's 2D model for stage 2 and stage 3 are plotted with dotted and dashed lines, respectively. In Fig. 12(b) the heights of the melt are plotted for both stages 2 and 3 with the same legend as that in Fig. 12(a). Both solutions show that as the block starts to melt a liquid layer is formed and it's height increases rapidly. This is because in the beginning the liquid layer is thin and does not offer the ice block good insulation, resulting in a quick melt. After approximately 10s the increase of liquid height slows. Toward the end of the melting process the block is smaller so there is less pressure pushing down on the liquid, as a result the liquid height increases more

rapidly.

The liquid height predicted by the 3D model is smaller than that of Myers's 2D model. A source of the error in Myers's model is that is assumes the problem to be 2D, when in fact the physical problem is 3D. The 2D model neglects the liquid leaking out from two of the four edges. This results in the 2D model having a thicker liquid layer. Near the end of the final stage both models have a rapid increase in liquid height. Toward the end of the melt process the 3D model has a thicker liquid height, because it melts more quickly. So at any particular time the 3D model will have more melt, as seen in Fig. 12(b).

In Figs. 13(a) and 13(b) the pressure distribution at mid-stage 2 and mid-stage 3 are plotted. The maximum pressure above atmospheric is approximately 900 Pa at $t = 57.67$s (mid-stage 2) and 200 Pa at $t = 416.5$s (mid-stage 3). The pressure clearly decreases as the block melts.

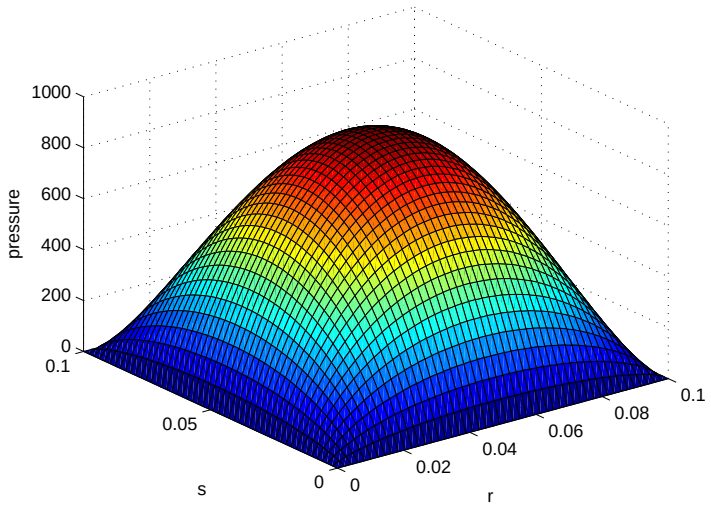

(a) Mid-stage 2: $t = 57.67$ s.

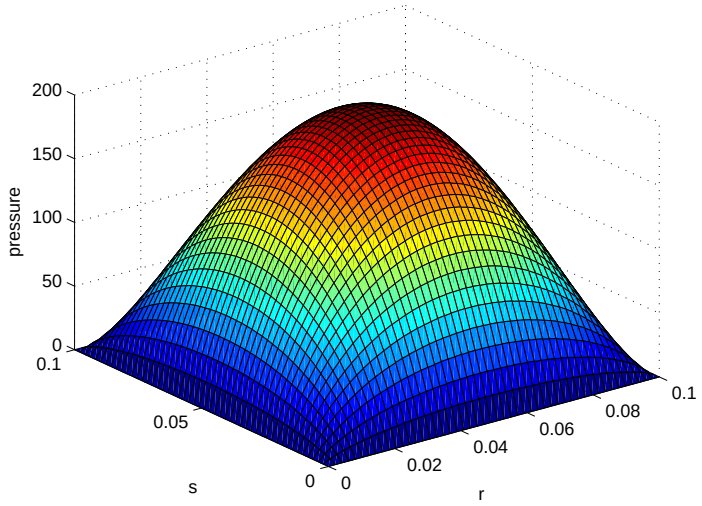

(b) Mid-stage 3: $t = 416.5$ s.

Figure 13: The distribution pressure is plotted in (a) and (b).

In Fig. 14 the temperature profile of the solid is at $t_2 = 115.35$s (end of stage 2, dashed line) and

$t_m/2 = 474.67$s (midway in the melting process, dotted line). The liquid profile is also plotted at these times (solid line), but it is difficult to see the liquid profiles in the plot as they lie very close to the axis. It is evident that the temperature in the solid increases as time progresses. In the time difference between the two plots, the block of ice has increased in temperature from approximately -15^oC to -2.5^oC. The plot at $t = 474.67$s (dotted line) does not extend past 0.025m suggesting that the block has melted to that height. The dashed line suggests that the block is approximately 0.044m high at $t = 115.35$s. The temperature profile of the liquid has a very steep gradient as a result of it's thin layer; the liquid layer is $h = 1.27 \times 10^{-4}$ m and $h = 1.56 \times 10^{-4}$ m at $t = 115.35$s and $t = 474.67$s, respectively. The temperature of the liquid at the substrate is at most 2^oC and at the top of the water layer is it 0^oC. The steep temperature gradient results from the fact that we have a temperature difference over a very thin water layer, i.e. $T_z \sim \triangle T/h$, where $\triangle T \sim 2$ and $h \sim 10^{-4}$. Since h is so small we have T_z large.

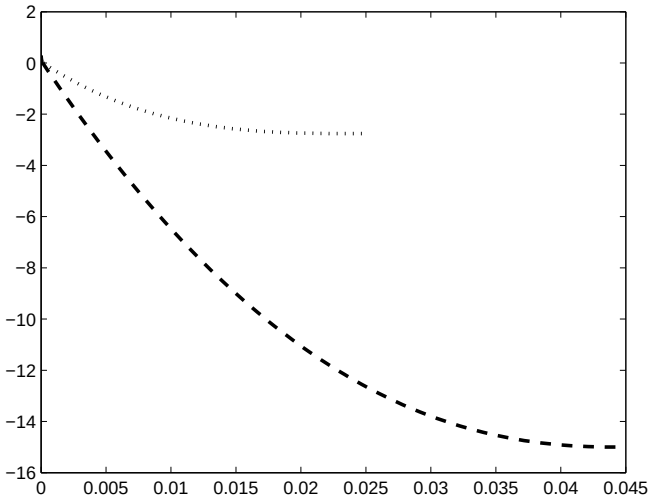

Figure 14: *The temperature in the solid at $t_m/2 = 474.67s$ (dotted line) and $t_2 = 110.5s$ (dashed line). The temperature in the liquid plotted at these times is close to the axis and difficult to see (solid line).*

5.6 Application to n-octadecane

In order to validate our 3D model we wish to compare it to the experimental results. The data is obtained from experiments carried out by Moallemi *et al.* [13] who worked with n-octadecane and developed an analytical expression for the height of the block, given by

$$H(t) = L\left[\left(\frac{H_0}{L}\right)^{3/4} - \frac{3\kappa_l t}{4L^2}\left\{\frac{gL^3}{\kappa_l^2}\left[\frac{c_l(T_0 - T_m)}{L_m + c_s(T_m - a)}\right]^3 \frac{\kappa_l}{4(\rho_s/\rho_l)^2\eta_l c_l}\right\}^{1/4}\right]^{4/3}. \tag{259}$$

Myers [19] also applied a 2D model to this set of experimental data and found a satisfying fit, but with a questionably high heat transfer coefficient of $h_{sl} = 7000W/m^2$. We wish to use our 3D model to obtain a good fit to the data, but with a more reasonable heat transfer coefficient. To be consistent with Myers's 2D model we take $h_{ss} = h_{sl}$, but run the 3D model with $h_{sl} = 3275W/m^2$.

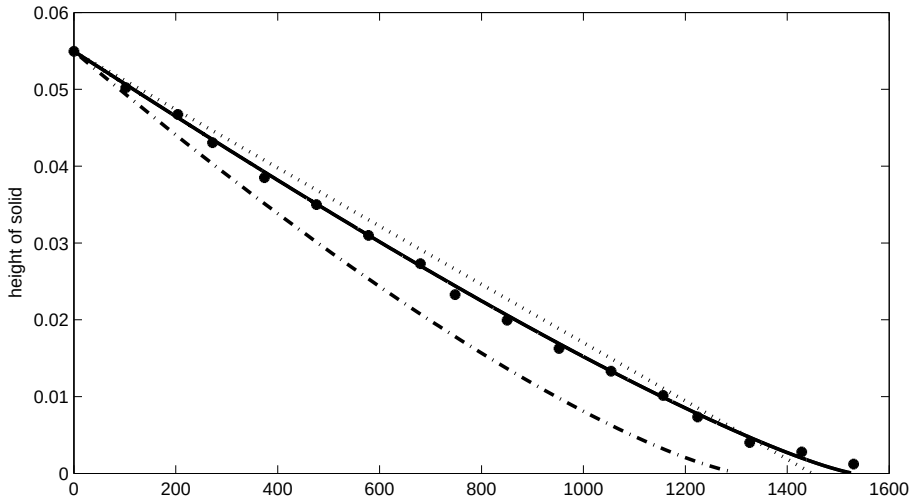

Figure 15: *The experimental data (asterisks) of $H(t)$ is compared to that of the 3D model with $h_{sl} = 3275W/m^2$ (solid line), Moallemi's analytical solution (dot-dashed line) and that of the quasi-steady solution (dotted line).*

In Fig. 5.6 the experimental data from [13] are marked with dots, the 3D model is shown as the solid line, Moallemi's analytical solution is the dot-dashed line and the quasi-steady solution is the dotted line. The approximate solution of Moallemi shows a melting rate higher than that of the experiment. A source of this problem is that Moallemi neglected the temperature gradient in the solid. The quasi-steady solution matches the experimental data well for small times, but since it assumes the solid to have a constant mass the melt rate is constant and so doesn't allow the $H(t)$ solution to curve with the experimental data. In our 3D model we have fluid leaking out in 2 dimensions, so we will have a thinner liquid layer which will result in a higher melting rate. In order to match the model to the experimental data we decrease the heat transfer coefficient from 7000W/m^2 to 3275W/m^2. This value of h_{sl} was chosen as it visibly gave us the best fit.

6 Conclusion

The goal of this dissertation was to develop an accurate, approximate solution method to describe the contact melting process. To achieve this we initially investigated approximate solutions for 1D Stefan problems. This allowed us to determine accurate solution methods through comparison with exact solutions and then subsequently apply these methods to problems with no exact solutions.

We started by dealing with the simple one dimensional heat transfer problem with constant boundary conditions, progressed to dealing with constant flux conditions, then moved onto solving the more complex one and two phase Stefan problems. We investigated a number of approximate methods and in each case we determined the most accurate solution. We applied our new found knowledge to a contact melting problem and finally, in order to validate our methodology, we compared the chosen minimal error approximation method with experimental data for the melting of n-octadecane.

In the one dimensional heat problem we compared the separable solution to that of the HBIM. We found that the separation of variable method is good for checking solutions on a finite domain for intermediate times. The HBIM proved to be more flexible so could be used for early and late times on any domain and it's efficiency could be improved, but when the separable solution was good it was better than the HBIM. As seen in §2.2 the HBIM did not perform well for a constant flux problem, which served as motivation to improve the method since we ultimately wanted to work with Stefan problems.

Applying the optimal HBIM, optimal RIM and CIM to the one phase Stefan problem we discovered that the best approximation method depended on the β value: for $\beta < 140$ the optimal RIM was preferred. In the case of large β values we also investigated perturbation methods to find the higher order perturbation method returned the lowest error for $\beta > 140$. Although the optimal RIM performed better than the optimal HBIM there was no proof that that would always be the case. For this reason we applied both methods to the two phase Stefan problem. Ultimately, both integral methods provided a satisfactory low error so we chose the optimal HBIM as our best method to apply to the contact melting problem due to the ease of its implementation.

Upon applying the optimal HBIM and using our three dimensional contact melting model we were able to prove our hypothesis correct. That is, we found that with a realistic heat transfer coefficient our model provided a good fit to the n-octadecane data. We owe this to the fact that the three dimensional model allowed the fluid to escape in four rather than two directions which resulted in a thinner liquid layer. As a result of this the liquid layer did not offer much insulation and the solid melted more rapidly which required us to decrease the heat transfer coefficient in order to maintain a good fit the experimental data.

References

[1] C. Clanet A. L. Biance and D. G. Quere. Leidenfrost drops. *Phys. Fluids*, 14, 2003.

[2] V. Alexiades and A. D. Solomon. *Mathematical Modeling of Melting and Freezing Processes.* Taylor and Francis, 1993.

[3] A. Antic and J.M. Hill. The double-diffusivity heat transfer model for grain stores incorporating microwave heating. *Appl. Math. Modelling*, 27: 629–647, 2003.

[4] A. Bejan. Contact melting heat transfer and lubrication. *Adv. Heat Transfer*, 24, 1994.

[5] A. Bejan. *Convection Heat Transfer, 3rd Edition.* Wiley, New Jersey, 2004.

[6] J. Caldwell and Y. Y. Kwan. On the perturbation method for the stefan problem with time-dependent boundary conditions. *Int. J. of Heat and Mass Transfer*, 46:14971501, 2003.

[7] J. Caldwell and Y. Y. Kwan. Numerical methods for one-dimensional Stefan problems. *Comm. Num. Methods Eng.*, 20: 535–545, 2004.

[8] A. Fowler. *Mathematical models in the applied sciences.* C.U.P, 1997.

[9] T. R. Goodman. The Heat-Balance Integral and Its Application to Problems Involving a Change of Phase. *Trans. ASME*, 80: 335–342, 1958.

[10] D. Groulx and M. Lacroix. Study of close contact melting of ice from a sliding heated flat plate. *Int. J. Heat Mass Trans.*, 19:44074416, 2006.

[11] H. Hong H. Yoo and C. Kim. Effects of transverse convection and solid-liquid density difference on the steady close-contact melting. *International Journal of Heat and Fluid Flow*, 19:368–373, 1998.

[12] J. M. Hill. *One-dimensional Stefan problems: an introduction.* Longman Scientific and Technical; New York, Wiley, 1987.

[13] B. W. Webb M. K. Moallemi and R. Viskanta. An experiemental and analytical study of close-contact melting. *International Journal of Heat Transfer*, 108:894, 1986.

[14] S. L. Mitchell and T. G Myers. Approximate solution methods for one-dimensional solidification from an incoming fluid. *App. Math. Comp.*, 202(1):311 – 326, 2008. DOI:10.1016/j.amc.2008.02.031.

[15] S. L. Mitchell and T. G. Myers. Application of standard and refined heat balance integral methods to one-dimensional Stefan problems. *SIAM Review*, 52(1):57–86, 2010. DOI. 10.1137/080733036.

[16] T. G. Myers. Optimizing the exponent in the heat balance and refined integral methods. *Int. Comm. Heat Mass Trans.*, 36(2):143–147, 2009, DOI:10.1016/j.icheatmasstransfer. 2008.10.013.

[17] T. G. Myers. Optimal exponent heat balance and refined integral methods applied to Stefan problems. *Int. J. Heat Mass Trans.*, 53, 2010 DOI:10.1016/j.ijheatmasstransfer.2009.10.045.

[18] T. G. Myers, S. L. Mitchell, G. Muchatibaya, and M. Y. Myers. A cubic heat balance integral method for one-dimensional melting of a finite thickness layer. *Int. J. Heat & Mass Trans.*, 50: 5305–5317, 2007.

[19] T.G. Myers, S.L. Mitchell, and G. Muchatibaya. Unsteady contact melting of a rectangular cross-section phase change material on a flat plate. *Phys. Fluids*, 20 103101, 2008 DOI:10.1063/1.2990751.

[20] P.M. Pavel and N. Ene. Planar solidification solution with mushy zone. *Energy Convers. Manage.*, 44:2977–2989, 2003.

[21] K. Pohlhausen. Zur naherungsweisen Integration der Differentialgleichunger der laminaren Grenzschicht. *Zeitschrift Math. Mech.*, 1: 252–258, 1921.

[22] A.S. Wood S. Kutluay and A. Esen. A heat balance integral solution of the thermistor problem with a modified electrical conductivity. *Appl. Math. Model.*, 30:386–394, 2006.

[23] N. Sadoun, E-K. Si-Ahmed, and P. Colinet. On the refined integral method for the one-phase Stefan problem with time-dependent boundary conditions. *App. Math. Modelling*, 30: 531–544, 2006.

[24] S.L. Mitchell T. G. Myers. Application of the combined integral method to stefan problems. *App. Math. Modelling*, In press, 2010.

[25] A. S. Wood. A new look at the heat balance integral method. *App. Math. Modelling*, 25(10): 815–824, 2001.

[26] D. G. Zill and M. R. Cullen. *Differential Equations with Boundary-Value Problems*. Brooks/Cole, 2005.